

A miR-124-mediated post-transcriptional mechanism controlling the cell fate switch of astrocytes to induced neurons

Elsa Papadimitriou,¹ Paraskevi N. Koutsoudaki,^{1,7,9} Irini Thanou,^{1,9} Dimitra Karagkouni,^{2,8,10} Timokratis Karamitros,^{3,10} Dafni Chroni-Tzartou,⁴ Maria Gaitanou,⁵ Christos Gkemis,¹ Maria Margariti,¹ Evangelia Xingi,⁶ Socrates J. Tzartos,⁴ Artemis G. Hatzigeorgiou,³ and Dimitra Thomaidou^{1,6,*}

¹Neural Stem Cells and Neuroimaging Group, Department of Neurobiology, Hellenic Pasteur Institute, Athens, Greece

²DIANA-Lab, Hellenic Pasteur Institute & Department of Computer Science and Biomedical Informatics, University of Thessaly, Larissa, Greece

³Bioinformatics and Applied Genomics Unit, Department of Microbiology, Hellenic Pasteur Institute, Athens, Greece

⁴Laboratory of Molecular Neurobiology and Immunology, Department of Neurobiology, Hellenic Pasteur Institute, Athens, Greece

⁵Laboratory of Cellular and Molecular Neurobiology – Stem Cells, Department of Neurobiology, Hellenic Pasteur Institute, Athens, Greece

⁶Light Microscopy Unit, Hellenic Pasteur Institute, Athens, Greece

⁷Present address: Molecular Carcinogenesis Group, Department of Histology and Embryology, Medical School, National and Kapodistrian University of Athens, Athens, Greece

⁸Present address: Department of Pathology, Harvard Medical School, Beth Israel Deaconess Medical Center, Broad Institute of MIT and Harvard, Boston, MA, USA

⁹These authors contributed equally

¹⁰These authors contributed equally

*Correspondence: thomaidou@pasteur.gr

<https://doi.org/10.1016/j.stemcr.2023.02.009>

SUMMARY

The microRNA (miRNA) miR-124 has been employed supplementary to neurogenic transcription factors (TFs) and other miRNAs to enhance direct neurogenic conversion. The aim of this study was to investigate whether miR-124 is sufficient to drive direct reprogramming of astrocytes to induced neurons (iNs) on its own and elucidate its independent mechanism of reprogramming action. Our data show that miR-124 is a potent driver of the reprogramming switch of astrocytes toward an immature neuronal fate by directly targeting the RNA-binding protein Zfp36L1 implicated in ARE-mediated mRNA decay and subsequently derepressing Zfp36L1 neurogenic interactome. To this end, miR-124 contribution in iNs' production largely recapitulates endogenous neurogenesis pathways, being further enhanced upon addition of the neurogenic compound ISX9, which greatly improves iNs' differentiation and functional maturation. Importantly, miR-124 is potent in guiding direct conversion of reactive astrocytes to immature iNs *in vivo* following cortical trauma, while ISX9 supplementation confers a survival advantage to newly produced iNs.

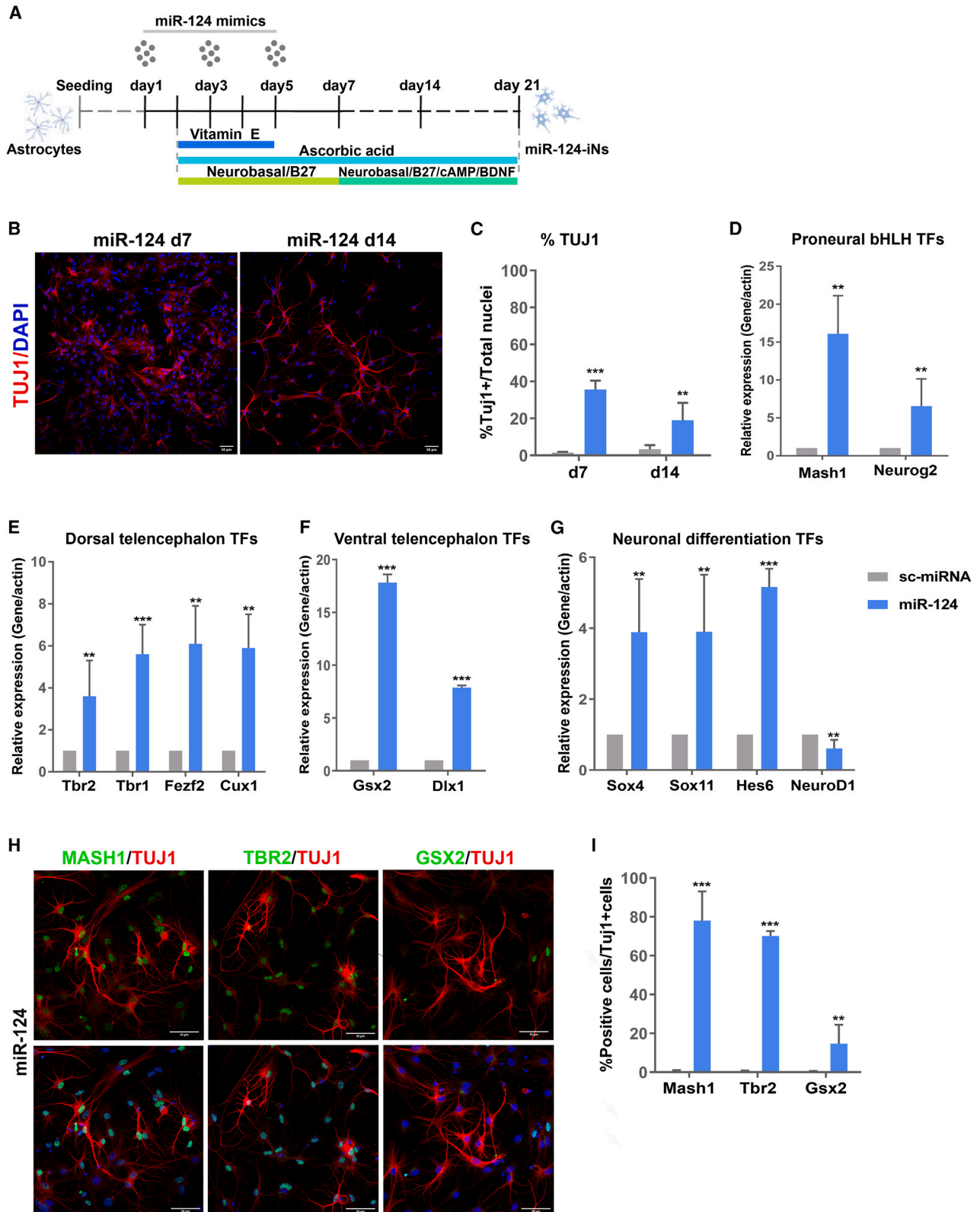
INTRODUCTION

Direct astrocytic reprogramming to induced neurons (iNs) is a powerful approach for manipulating cell fate, as it takes advantage of the intrinsic neural stem cell (NSC) potential of brain-resident reactive astrocytes. To this end, astrocytic cell fate conversion to iNs has been well established *in vitro* (Heinrich et al., 2010; Aravantinou-Fatorou et al., 2015) and *in vivo* (Guo et al., 2014; Mattugini et al., 2019) using combinations of transcription factors (TFs) or chemical cocktails (Gao et al., 2017). Challenging the expression of lineage-specific TFs is accompanied by changes in the expression of microRNAs (miRNAs), which post-transcriptionally modulate high numbers of neurogenesis-promoting factors and have therefore been introduced, supplementary or alternatively to TFs, to instruct direct neuronal reprogramming (Yoo et al., 2011).

Among neurogenic miRNAs, miR-124 has been shown to contribute to efficient neurogenic conversion of fibroblasts when coupled with certain TFs or other miRNAs, in particular miR-9/9*, and the reprogramming potential of this cocktail has been elaborately studied at the tran-

scriptomic and epigenetic levels (Abernathy et al., 2017; Victor et al., 2014). miR-124 acts globally to increase the expression levels of neuronal genes by repressing components of major neuronal gene repressor complexes, such as REST (Volvert et al., 2014) and the Polycomb Repressive Complex 2 (Neo et al., 2014), while it also participates at the post-transcriptional regulation of neuronal transcripts by targeting the neuron-specific splicing global repressor PTBP1 (Makeyev et al., 2007). Besides its roles in transcriptional and post-transcriptional regulation, miR-124 is a key mediator of a chromatin permissive environment for neuronal reprogramming through its involvement in the formation of the neuron-specific chromatin remodeling complex, nBAF (Yoo et al., 2009).

However, although miR-124 has been utilized in reprogramming cocktails for the neurogenic conversion of fibroblasts (Birtele et al., 2019; Victor et al., 2018), neither its potential to induce fate conversion of astrocytes to iNs *in vitro* or *in vivo* nor its independent mechanism of direct reprogramming action have been investigated. In this study, we show that miR-124 is sufficient to instruct



(legend on next page)



reprogramming of cortical astrocytes to immature iNs *in vitro*, controlling their reprogramming “switch” toward the neuronal fate by downregulating genes with important regulatory roles in astrocytic function. Among these, we identified for the first time the RNA-binding protein ZFP36L1, implicated in ARE-mediated mRNA decay (Lai et al., 2000) as a direct target of miR-124, and further found neuronal-specific ZFP36L1 targets involved in cortical development being derepressed in miR-124-iNs. Importantly, by blocking miR-124 binding in *Zfp36L1* 3' UTR, we revealed that miR-124/*Zfp36L1* interaction is one of the drivers of miR-124-induced astrocytic fate switch and induction of neuronal identity. To enhance the neuronal differentiation of reprogrammed immature iNs, we combined miR-124 with isoexasole-9 (ISX9), a chemical compound known to possess neurogenesis-promoting properties (Li et al., 2015; Schneider et al., 2008). Functional analysis of the two molecules' combination revealed that *in vitro* addition of ISX9 both promoted the neurogenic conversion and greatly enhanced the functional maturation of miR-124 + ISX9-iNs. Importantly, *in vivo* miR-124 was also potent, either alone or along with ISX9, in guiding neuronal reprogramming of reactive astrocytes following cortical trauma to immature iNs, present after 8 weeks, with ISX9 contributing to iNs' enhanced survival, revealing the *in vivo* “master” reprogramming capacity of miR-124 within the injured cortical microenvironment.

RESULTS

miR-124 is sufficient to instruct reprogramming of postnatal cortical astrocytes to immature induced neurons

To study the potential of miR-124 to instruct neuronal reprogramming of astrocytes on its own, cultured postnatal day 3–5 mouse cortical astrocytes were transfected with miR-124-3p mimics (Figure 1A). First, we verified that the initial primary astrocytic culture comprised mainly GFAP⁺ astrocytes (72.2%) while only 2.3% were TUJ1⁺ neurons (Figures S1A and S1B). After verifying that almost 70% of astrocytes were transfected with one round of miRNA-Dy546

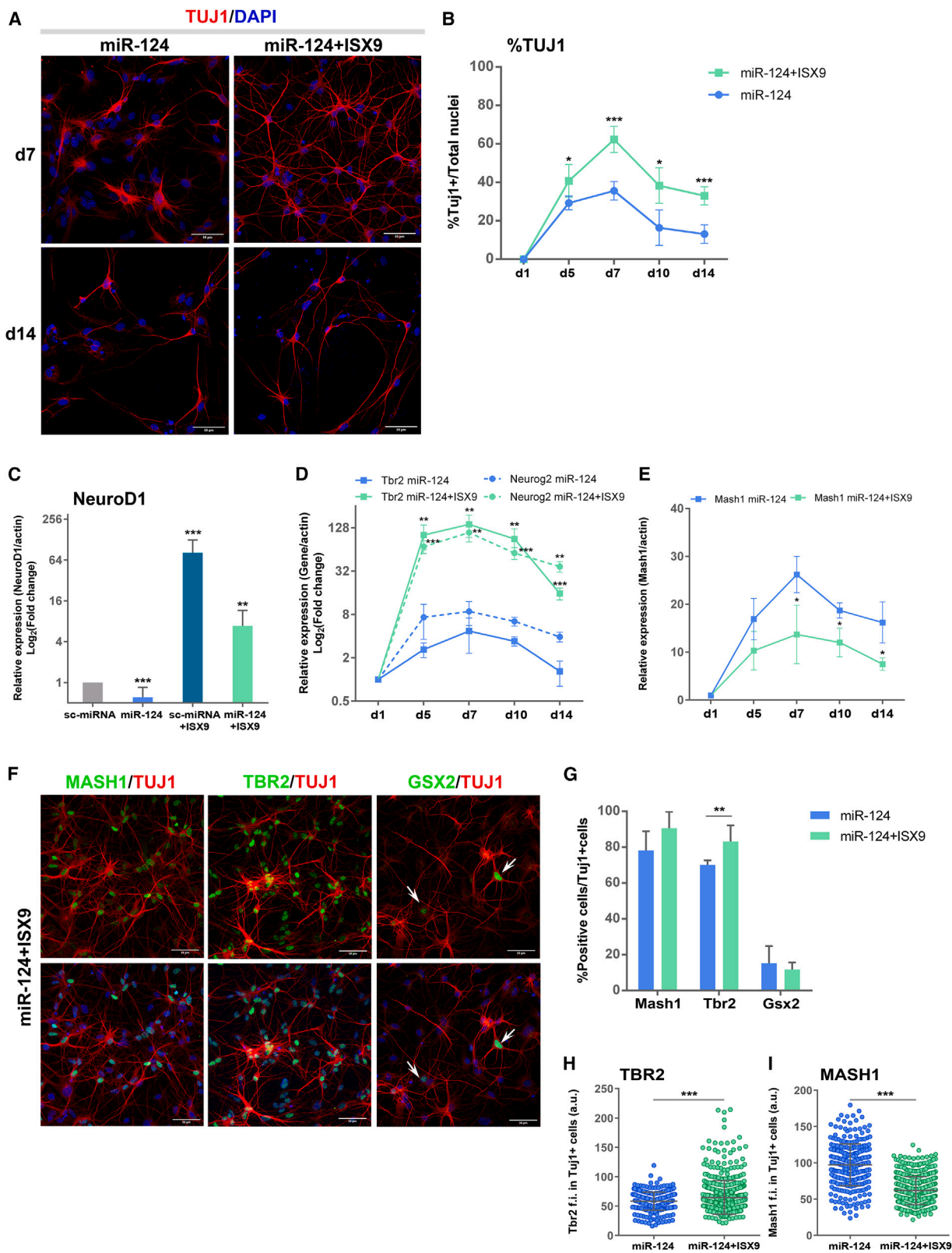
mimics (Figures S1C and S1D), we established a protocol of three transfections with miR-124 mimics, which after 1 week (day 7) led to the highest percentage of TUJ1⁺ cells (nearly 35%) exhibiting a multipolar morphology with fine processes (Figures 1B, 1C, and S1E). Bromodeoxyuridine (BrdU) administration for the first 4 days of reprogramming revealed that overexpression of miR-124 significantly reduced the percentage of proliferating astrocytes from 70% to 50% at day 7 (Figures S1F and S1G), while almost 60% of TUJ1⁺ cells had incorporated BrdU (Figure S1H), indicating their non-neuronal origin. In addition, miR-124-iNs exhibited low differentiation potential and only 19% of cells remained TUJ1⁺ at day 14 (Figures 1B and 1C). The ability of miR-124 to instruct neurogenic reprogramming was further supported by qRT-PCR analysis of several neurogenic TFs at day 7, when miR-124 overexpression induced the upregulation of mRNA levels of the proneural TFs *Mash1* and *Neurog2* to a lesser extent (Figure 1D), while it upregulated TFs related to both dorsal (Figure 1E) and ventral telencephalic development (Figure 1F). We also observed upregulation of TFs related to neuronal differentiation (Figure 1G), although we failed to detect upregulation of *NeuroD1* (Figure 1G), which is known to play a crucial role in neuronal reprogramming (Guo et al., 2014; Matsuda et al., 2019). Instead, miR-124 significantly reduced *NeuroD1* mRNA levels, implying that this reduction may contribute to the low differentiation capacity of miR-124-iNs. Furthermore, immunofluorescence analysis at day 7 indicated that the majority of miR-124-iNs (nearly 80%) were MASH1⁺ and also exhibited low TBR2 expression (nearly 70%), while only a small percentage of iNs (15%) were positive for the ventral TF GSX2 (Figures 1H and 1I). Interestingly, almost all miR-124-iNs were double-positive for MASH1 and TBR2 (Figure S1I), indicating that a MASH1-TBR2 trajectory is most prominently activated in the majority of miR-124-iNs.

The neurogenic compound ISX9 greatly enhances the miR-124-induced reprogramming efficiency and differentiation state of iNs

The downregulation of *NeuroD1* by miR-124 prompted us to supplement the reprogramming medium from day 2 to day

Figure 1. miR-124 is sufficient to instruct reprogramming of postnatal cortical astrocytes to iNs

- (A) Overview of the miR-124-mediated reprogramming protocol.
 (B) Immunostaining of astrocytes reprogrammed with miR-124 at day 7 and day 14 of the reprogramming protocol with anti-TUJ1 antibody.
 (C) Quantification of the percentage of TUJ1⁺ reprogrammed cells (n = 4 independent experiments).
 (D–G) qRT-PCR analysis of the mRNA levels of the proneural TFs *Mash1* and *Neurog2* (D), the dorsal telencephalon TFs *Tbr2*, *Tbr1*, *Fezf2*, and *Cux1* (E), the ventral telencephalon TFs *Gsx2* and *Dlx1* (F), and the neuronal differentiation TFs *Sox4*, *Sox11*, *Hes6*, and *NeuroD1* (G). Data are presented as fold change vs. sc-miRNA (n = 3 independent experiments).
 (H) Co-immunostaining of astrocytes reprogrammed with miR-124 at day 7 with anti-MASH1/TUJ1, anti-TBR2/TUJ1, and anti-GSX2/TUJ1 antibodies.
 (I) Quantification of the percentage of MASH1⁺, TBR2⁺, and GSX2⁺ in TUJ1⁺ reprogrammed cells (n = 3 independent experiments).
 p < 0.01, *p < 0.001 vs. sc-miRNA. Scale bars, 50 μ m.



(legend on next page)



10 with the chemical compound ISX9, known to upregulate *NeuroD1* levels and enhance neuronal differentiation (Schneider et al., 2008). Indeed, ISX9 addition led to the acquisition of a more differentiated neuronal phenotype with a smaller soma and longer projections (Figure 2A) and significantly increased the percentage of TUJ1⁺ iNs from 35% to 62% at day 7 and from 19% to 38% at day 14 (Figure 2B). Importantly, ISX9 was potent in reversing the miR-124-induced reduction of *NeuroD1* mRNA levels (Figure 2C) and greatly elevating the transcriptional levels of *Neurog2* and *Tbr2* peaking at day 7 (Figure 2D), while it also induced a moderate reduction in *Mash1* mRNA levels (Figure 2E). Importantly, ISX9 was not able to induce reprogramming of astrocytes on its own (single-cell [sc]-miRNA + ISX9) (Figure S2A), despite evoking robust upregulation of the mRNA levels of *NeuroD1* (Figure 2D) and other neurogenic TFs (Figure S2B) and to a small, but significant, extent the protein levels of MASH1 and TBR2 (Figures S2C and S2D). Additionally, supplementation of ISX9 along with miR-124 significantly increased the percentage of TBR2⁺/TUJ1⁺ iNs without affecting the percentages of MASH1⁺/TUJ1⁺ iNs or GSX2⁺/TUJ1⁺ iNs relative to miR-124 alone (Figures 2F and 2G). Moreover, measurement of mean nuclear fluorescence intensity of miR-124-iNs and miR-124 + ISX9-iNs at day 7 revealed a significant enhancement of TBR2 (Figure 2H) and a reduction of MASH1 protein levels (Figure 2I) following ISX9 addition.

These results led us to the inference that addition of ISX9 in the reprogramming medium reinforces the passage of miR-124 + ISX9-iNs through a TBR2⁺ intermediate stage, which seems to be the main reprogramming route that these iNs follow. Interestingly, the addition of ISX9 also significantly enhanced the expression of *Insm1* (Figure S2E), a key transcriptional regulator of intermediate progenitors (IPs) (Elsen et al., 2018), further supporting

the notion that iNs pass through an intermediate stage bearing molecular characteristics of endogenous IPs.

miR-124 + ISX9-iNs exhibit characteristics of mature, electrophysiologically active neurons

The majority of miR-124-iNs and miR-124 + ISX9-iNs were positive for the cortical TF TBR1 at day 14 (Figures S2F and S2G). We mainly observed a moderate nuclear TBR1 expression in miR-124-iNs, whereas miR-124 + ISX9-iNs exhibited strong cytoplasmic TBR1 expression besides a moderate nuclear one (Figure S2F), a finding previously reported in cortical neurons (Hong and Hsueh, 2007). After day 21 nearly 80% of TUJ1⁺ miR-124 + ISX9-iNs were also positive for the mature neuronal markers MAP2 and SYNAPSIN1, exhibiting a differentiated neuronal morphology (Figures 3A and 3B), whereas miR-124-iNs did not exhibit signs of further maturation and only few of them were MAP2⁺ and SYNAPSIN1⁺ (Figure 3B). Additionally, at day 28 nearly 90% of miR-124 + ISX9-iNs were positive for the glutamatergic marker VGlut1 (Figures 3C and 3D), while only 12% of them were GABA⁺ (Figures 3D and S2H).

To establish the functional maturation of miR-124-iNs and miR-124 + ISX9-iNs, we performed electrophysiological analysis with whole-cell voltage-clamp and current-clamp recordings at days 15–27. Rapidly inactivating inward Na⁺ currents and persistent outward K⁺ currents were recorded in miR-124 + ISX9-iNs after day 22 (n = 47/80 cells) in response to depolarizing voltage steps, while further application of tetrodotoxin (TTX) and tetraethylammonium (TEA)—selective Na⁺ channel (Na_v) and K⁺ channel (K_v) blockers, respectively—confirmed that the Na_v were responsible for the inward currents and K_v for the outward currents (Figure 3E). A small amount of K_v channels appeared in miR-124 + ISX9-iNs before day 21, while they became more evident from day 23 to day 27

Figure 2. The neurogenic compound ISX9 greatly enhances the miR-124-induced reprogramming efficiency and differentiation state of iNs

(A) Immunostaining of astrocytes reprogrammed with miR-124 or miR-124 + ISX9 at day 7 and day 14 with anti-TUJ1 antibody.
 (B) Quantification of the percentage of TUJ1⁺ cells at days 1, 5, 7, 10, and 14 (n = 3 independent experiments for day 5 and day 10, n = 8 for day 7, and n = 4 for day 14; *p < 0.05, ***p < 0.001 vs. miR-124).
 (C) qRT-PCR analysis of the mRNA levels of *NeuroD1* at day 7. Data are presented as log₂ (fold change) vs. sc-miRNA (n = 3 independent experiments; **p < 0.01, ***p < 0.001 vs. sc-miRNA).
 (D and E) qRT-PCR analysis of the mRNA levels of the TFs, *Neurog2* and *Tbr2* (D) and *Mash1* (E) at days 1, 5, 7, 10, and 14. Data are presented as log₂ (fold change) (D) and fold change (E) vs. astrocytes (day 1) (n = 3 independent experiments; *p < 0.05, **p < 0.01, ***p < 0.001 vs. miR-124).
 (F) Co-immunostaining of astrocytes reprogrammed with miR-124 + ISX9 at day 7 with anti-MASH1/TUJ1, anti-TBR2/TUJ1, and anti-GSX2/TUJ1 antibodies.
 (G) Quantification of the percentage of MASH1⁺, TBR2⁺, and GSX2⁺ in TUJ1⁺ iNs reprogrammed either with miR-124 or miR-124 + ISX9 at day 7 (n = 3 independent experiments; **p < 0.01 vs. miR-124).
 (H and I) Measurement of the mean nuclear fluorescence intensity of TBR2 (H) and MASH1 (I) in TUJ1⁺ iNs reprogrammed either with miR-124 or miR-124 + ISX9 at day 7 (co-immunostaining with anti-TBR2/MASH1/TUJ1 antibodies). A representative experiment is shown of n = 3 independent experiments (n = 326 cells for miR-124 and n = 540 cells for miR-124 + ISX9; ***p < 0.001 vs. miR-124).
 Scale bars, 50 μm.

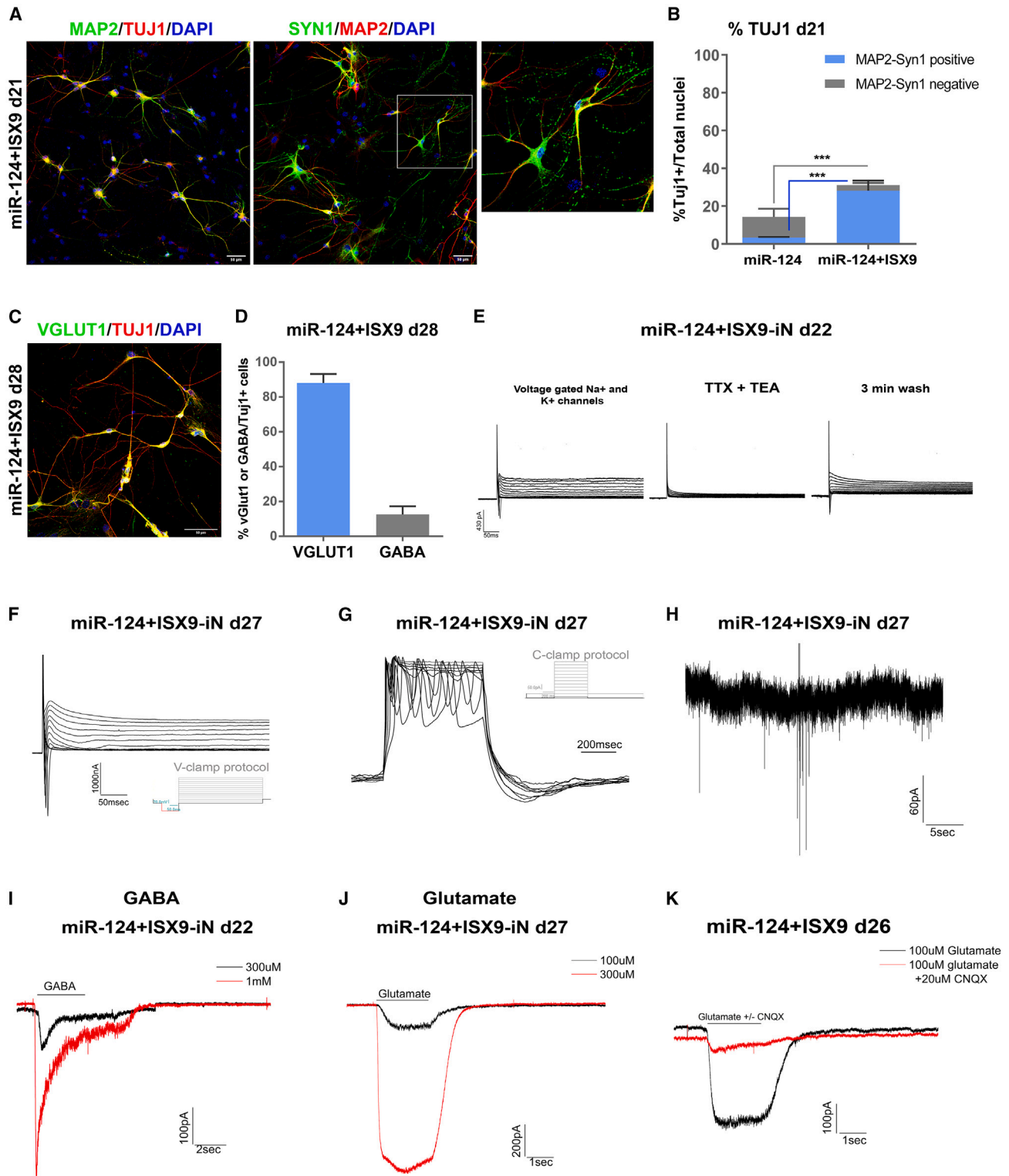


Figure 3. miR-124 + ISX9-iNs exhibit characteristics of mature, electrophysiologically active neurons

(A) Co-immunostaining of miR-124 + ISX9-iNs at day 21 with anti-MAP2/TUJ1 and anti-MAP2/SYN1 antibodies.

(B) Quantification of the percentage of TUJ1⁺ miR-124-iNs and miR-124 + ISX9-iNs at day 21. The percentage of MAP2/SYN1 double-positive (DP) TUJ1⁺ iNs is shown in blue (n = 3 independent experiments; ***p < 0.001).

(legend continued on next page)



(Figure 3F), in accordance with the ability of almost all recorded miR-124 + ISX9-iNs ($n = 21/30$ cells) to generate repetitive action potentials (APs) upon membrane depolarization (Figure 3G). The current-clamp recording spikes of miR-124 + ISX9-iNs were less sharp and frequent in relation to more mature iNs reported in other studies (Li et al., 2015), possibly due to the presence of lower amounts of Na_V and K_V , which were, however, sufficient for the generation of APs. Finally, rare spontaneous postsynaptic current activity was detected in few mature miR-124 + ISX9-iNs (day 27) (Figure 3H). On the other hand, miR-124-iNs exhibited lower amounts of Na_V and K_V channels and were thus not capable of firing APs ($n = 15$ cells).

The majority (80%) of miR-124 + ISX9-iNs were capable of responding to different concentrations of GABA early during their maturation (day 22) (Figure 3I) even before the appearance of APs, which is in compliance with the expression of GABA receptors in early stages of neuronal development (Luján et al., 2005). Additionally, miR-124 + ISX9-iNs were responding to L-glutamate in a concentration-dependent manner (Figure 3J), while L-glutamate-sensitive inward current was completely blocked after co-application of 100 μM L-glutamate and 20 μM cyanquinoxaline (CNQX), indicating the presence of AMPA/kainite receptors (Figure 3K).

miR-124 and ISX9 exhibit both independent and cooperative transcriptional contributions in the reprogramming process to iNs

To analyze in depth the molecular mechanism through which miR-124 contributes to the reprogramming process either alone or following ISX9 supplementation, we performed RNA sequencing (RNA-seq) of miR-124-iNs and miR-124 + ISX9-iNs at day 7, using as controls astrocytes obtained on the initial day of the reprogramming (day 1) and sc-miRNA transfected astrocytes at day 7. The differential expression analysis was performed between

day-7 miR-124-iNs or miR-124 + ISX9-iNs and day-1 astrocytes (astro) (Figure 4) to uncover the whole spectrum of transcriptional changes occurring during neurogenic reprogramming of initiating astrocytes (miR-124-iNs vs. astro and miR-124 + ISX9-iNs vs. astro, respectively), whereas the day-7 sc-miRNA-transfected astrocytes (sc-miRNA astro) were used as the ultimate control for the identification of miR-124 target genes (see Figure 5).

We identified 4,233 differentially expressed genes (DEGs) in miR-124-iNs vs. astro and 6,652 DEGs in miR-124 + ISX9-iNs vs. astro ($1 \leq \log_2(\text{fold change}) \leq -1$, false discovery rate [FDR] < 0.05) (Figure S3A). Heatmap analysis of DEGs (miR-124-iNs vs. astro and miR-124 + ISX9-iNs vs. astro) (Figure 4A) indicated that miR-124 alone efficiently downregulated a cluster enriched in astrocytic genes (cluster I). At the same time miR-124 upregulated a cluster of neuronal-specific genes (cluster III), many of which were further upregulated by ISX9 supplementation, while ISX9 highly upregulated a neuronal-specific cluster (cluster II) that was most exclusively expressed in miR-124 + ISX9-iNs.

Gene ontology (GO) enrichment analysis of biological processes for the upregulated DEGs of both miR-124-iNs vs. astro and miR-124 + ISX9-iNs vs. astro further revealed that miR-124 alone upregulated genes related to generation of neurons and neuronal differentiation as well as to more specific neuronal functions mostly associated with synaptic transmission (Figure 4B, orange), while ISX9 greatly enhanced the number of upregulated genes related to more mature neuronal functions such as AP, axon development, and subtype-specific synaptic transmission (Figure 4B, red). Furthermore, enrichment analysis of the downregulated DEGs of miR-124-iNs vs. astro indicated that many of them were related to cell cycle, gliogenesis, and astrocyte differentiation (Figure 4C). Interestingly, this analysis revealed a strong effect of miR-124 in downregulating components of many signaling pathways,

(C) Co-immunostaining of miR-124 + ISX9-iNs at day 28 with anti-vGLUT1/TUJ1 antibodies.

(D) Quantification of the percentage of $\text{VGlut1}^+/\text{TUJ1}^+$ and $\text{GABA}^+/\text{TUJ1}^+$ miR-124 + ISX9-iNs at day 28 ($n = 3$ independent experiments).

(E) Superimposed traces of inward Na^+ and outward K^+ currents evoked by depolarizing voltage steps obtained from an miR-124 + ISX9-iN (day 22) (left panel). Inhibition of both inward and outward currents after 1 min pre-application of 1 μM TTX + 10 mM TEA (middle panel), followed by full recovery of the current traces after a 3-min wash (right panel).

(F) Superimposed traces of inward Na^+ and outward K^+ currents evoked by depolarizing voltage steps obtained from an miR-124 + ISX9-iN (day 27).

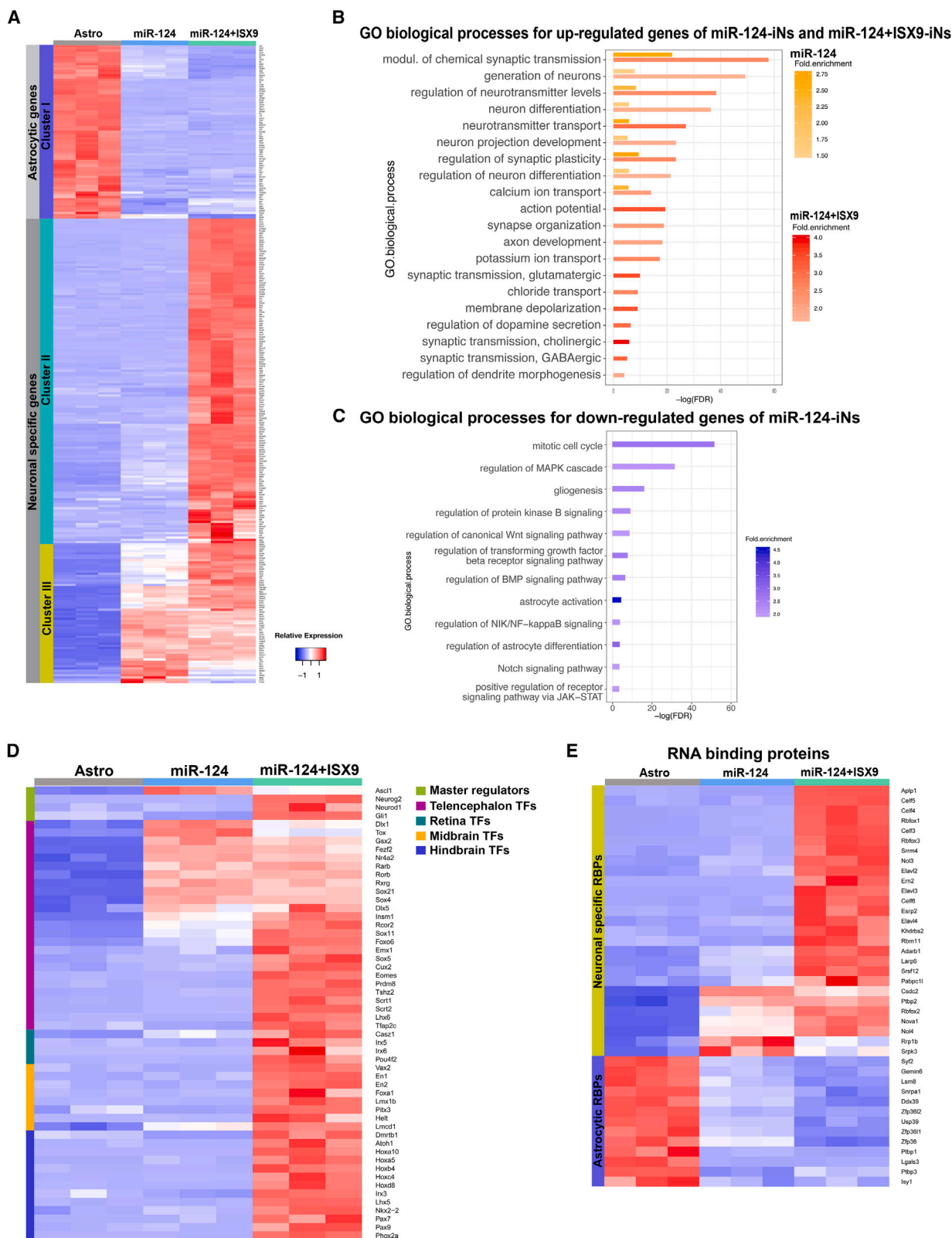
(G) Repetitive action potential induced from a mature miR-124 + ISX9-iN (day 27) by different current steps at the current-clamp mode.

(H) Mature miR-124 + ISX9-iN (day 27) exhibiting spontaneous postsynaptic activity at -70 mV holding potential.

(I and J) Representative traces of ionic currents induced by application of GABA in two concentrations (300 μM and 1 mM) in an miR-124 + ISX9-iN at early stage of neuronal maturation (day 22) (I) and glutamate in two concentrations (100 μM and 300 μM) from a miR-124 + ISX9-iN at a later stage of maturation (day 27) (J).

(K) Superimposed traces of a mature miR-124 + ISX9-iN (day 26) with application of 100 μM glutamate (Glut) or co-application of 100 μM Glut + 20 μM CNQX indicate that the antagonist CNQX inhibits the AMPA/kainite glutamate receptor. The cell membrane potential was held at -70 mV, and the time of agonist application is indicated in bars above the traces.

Scale bars, 50 μm .



(legend on next page)



including MAPK, PKB, canonical WNT, TGF- β , BMP, NOTCH, and JAK/STAT (Figure 4C), known to play important roles in astrocytic identity and function (Acas-Fonseca et al., 2019; Yang et al., 2012).

Since reprogramming is a process that implicates great changes in the transcriptomic, post-transcriptomic, and epigenetic landscape of *trans*-differentiating cells, we sought to identify the differentially expressed TFs, epigenetic factors (EFs), and RNA-binding proteins (RBPs) in our datasets that could possibly drive the reprogramming process. Heatmap analysis of astrocytic TFs (Figure S3B) indicated that miR-124 potently downregulated TFs related to astrocytic function such as *Id1*, *Id3*, *Tcf4*, *Tcf7l1*, *Rbpj*, and *Nfic*, while the addition of ISX9 exhibited a minor contribution to their downregulation (Figure S3B). Validation of many of those genes with qRT-PCR verified the observed trend and also indicated that ISX9 alone (sc-miRNA + ISX9) failed to downregulate their mRNA levels (Figure S3C). In parallel, heatmap analysis of upregulated neuronal-specific TFs revealed that miR-124 upregulated TFs related to telencephalic development such as *Tox*, *Foxo6*, *Scrt1*, *Scrt2*, and *Rcor2* (Figure 4D), along with TFs that we had already identified through prior qRT-PCR analysis (*Mash1*, *Insm1*, *Hes6*, *Sox4*, *Fezf2*, *Gsx2*, and *Dlx1*). ISX9 increased the number of TFs implicated in telencephalic development, among which were *Eomes* (*Tbr2*), *Prdm8*, *Ovol2*, *Tfap2c*, and *Tshz2* (Figure 4D), but unexpectedly it also highly upregulated TFs related to more ventral/caudal brain regions, such as the retina, midbrain, and hindbrain/spinal cord (Figure 4D), possibly implying that ISX9 expands region-specific neuronal identity at the transcriptional level. Validation of selected TFs/EFs expressed either in telencephalon (Figure S3D) or midbrain (Figure S3E) and hindbrain/spinal cord (Figure S3F) by qRT-PCR verified their upregulation by ISX9.

Interestingly, heatmap analysis of differentially expressed RBPs revealed that miR-124 was sufficient to downregulate many RBPs expressed in astrocytes such as the splicing factors *Ptbp1*, *Snrpa1*, *Lgals3*, and *Isy1* and the mRNA decay proteins *Zfp36*, *Zfp36L1*, and *Zfp36L2* (Figure 4E). In addition, miR-124 moderately upregulated

neuronal-specific RBPs, among which were *Elavl2*, *Elavl4*, *Nova1*, *Rbfox1*, *Rbfox2*, *Celf3*, and *Nol3*, while ISX9 induced their further upregulation and significantly increased the number of neuron-specific RBPs such as *Aplp1*, *Celf4*, *Celf5*, *Celf6*, *Elavl3*, *Ern2*, *Esrp2*, and *Rbfox3* (Figure 4E).

The analysis of differentially expressed EFs revealed that miR-124 increased the levels of several EFs related to epigenetic transcriptional activation, including *Kmt2c*, *Tet1*, *Smarca1*, *Smarca2*, *Chd7*, and *Ss18L1* (*Crest*) (Figure S3G). ISX9 further contributed in upregulating *Chd5*, *Actl6b*, *Dpf3*, and *Smyd3*, while interestingly it majorly contributed in downregulating EFs related to epigenetic transcriptional repression, such as *Suv39h1*, *Suv39h2*, *Hdac5*, and *Hdac7* (Figure S3G).

Importantly, comparison of our RNA-seq datasets with publicly available scRNA-seq data from embryonic mouse cortex (Ruan et al., 2021) revealed that miR-124 initiates a transcriptional program characteristic of endogenous intermediate progenitor cells (IPCs) (Figures S3H and S3I), while ISX9 enhances neuronal differentiation of miR-124-iNs toward layer-specific neuronal gene signatures (Figures S3H–S3J).

The non-neuronal RBP ZFP36L1 is a novel direct target of miR-124

To obtain a closer insight into the post-transcriptional effects of miR-124 on the astrocytic transcriptome, we sought to determine the direct targets of miR-124 that could act as drivers of the reprogramming switch. To this end, we utilized publicly available Ago HITS-CLIP data from mouse brain cortex (Chi et al., 2009) in order to detect miR-124 binding sites. The analysis revealed 171 direct targets of miR-124, also defined as downregulated in the miR-124-iNs vs. sc-miRNA astro RNA-seq analysis ($\log_2(\text{fold change}) \leq -1$, FDR < 0.01). miR-124 targets were subsequently filtered to examine genes expressed in astrocytes, utilizing a published reference list for expressed transcripts in distinct cell types of the mouse brain (Zhang et al., 2014), ending up with 130 miR-124 direct target genes (Figure 5A). Interestingly, among these genes we identified the known targets of miR-124, *Sox9* and *Lhx2*, but failed to detect

Figure 4. RNA-seq analysis revealed both independent and cooperative transcriptional contributions of miR-124 and ISX9 in the reprogramming process

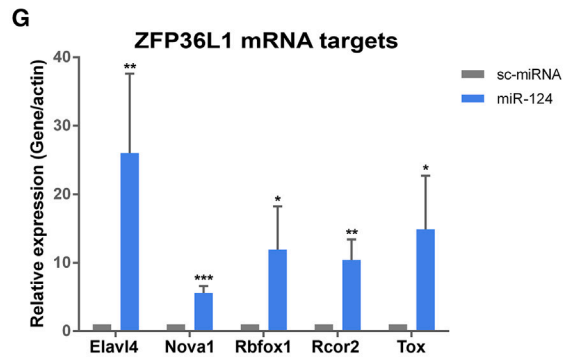
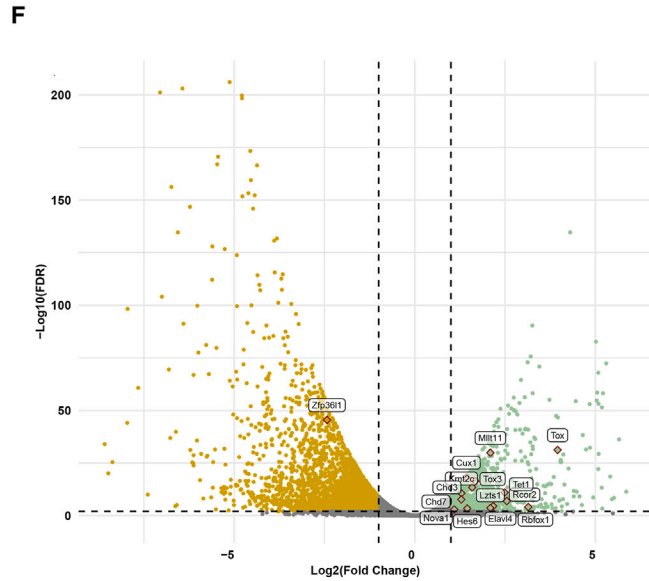
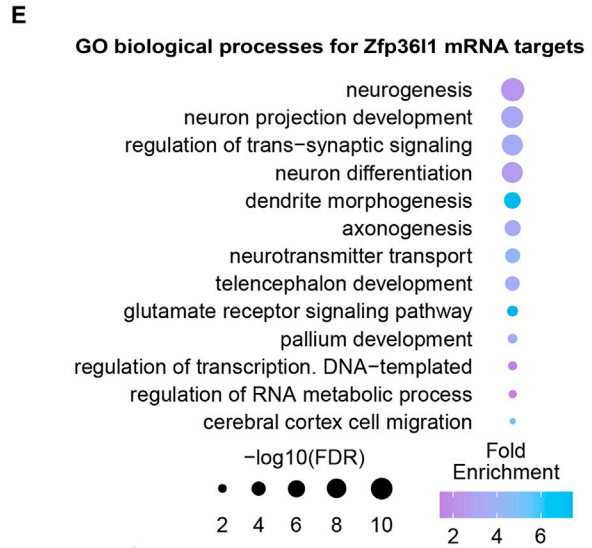
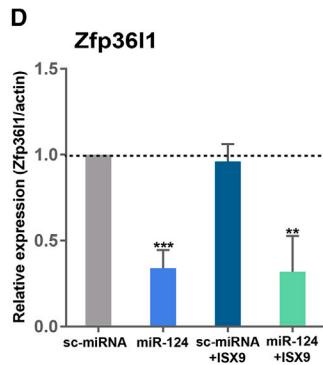
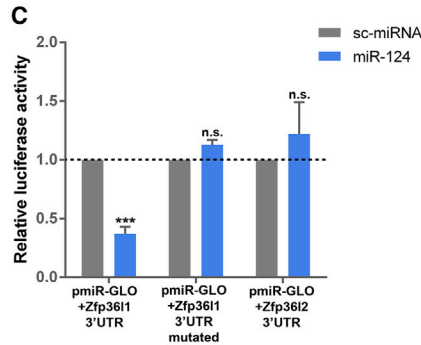
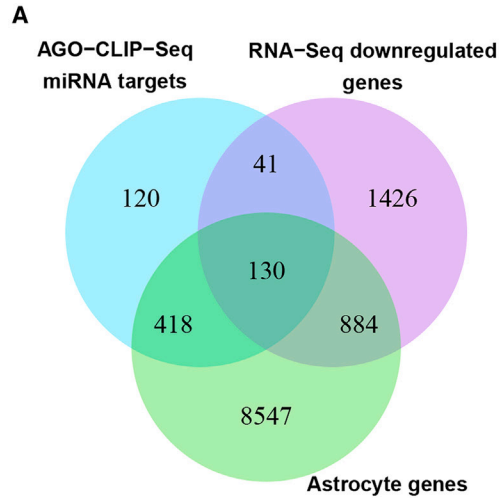
(A) Heatmap analysis of 300 up- and downregulated DEGs that belong to the GO terms Glial cell differentiation, Gliogenesis, Astrocyte development, Generation of neurons, Neuron differentiation, Regulation of neuron differentiation, Neurotransmitter transport, and Synaptic signaling.

(B) GO analysis of biological processes for the upregulated DEGs in miR-124-iNs vs. astro (orange) and miR-124 + ISX9-iNs vs. astro (red).

(C) GO analysis of biological processes for the downregulated DEGs in miR-124-iNs vs. astro. GO terms are ranked according to $\log_{10}(\text{FDR})$, and the intensity legends indicate the fold enrichment of each GO term.

(D) Heatmap analysis of 54 upregulated differentially expressed TFs clustered according to the brain region where they are developmentally expressed (telencephalon, retina, midbrain, and hindbrain).

(E) Heatmap analysis of 40 up- and downregulated RBPs.



(legend on next page)



Ptbp1 and *Scp1*, which are well-characterized miR-124 targets with a prominent role in neurogenic reprogramming.

In search of novel miR-124 targets with a regulatory role, a prominent target was the RBP ZFP36L1, implicated in mRNA decay (Lai et al., 2000) and highly expressed in cortical glial cells (Weng et al., 2019), cortical radial glial precursors (Weng et al., 2019; Yuzwa et al., 2017), and other non-neuronal cells (Carrick and Blackshear, 2007). miR-124 directly binds to the 3' UTR of *Zfp36L1* transcript with perfect seed complementarity (7mer-m8 site) (Figure 5B), while in reanalysis of publicly available Ago HITS-CLIP data from human motor cortex and cingulate gyrus tissues, the miR-124 binding site on the 3' UTR of *ZFP36L1* human transcript was found to be conserved (Figure 5B).

The targeting of this binding site in *Zfp36L1* 3' UTR by miR-124 was further validated by luciferase assays, where it was shown that its mutation completely blocked the strong downregulation of luciferase activity induced by miR-124 (Figures 5C, S4A, and S4B). Of note, miR-124 does not target the 3' UTR of *Zfp36L2*, predicted to contain two binding sites (Figures 5C, S4C, and S4D), further supporting its specificity on ZFP36L1 regulation. The efficient downregulation of *Zfp36L1* by miR-124 was also validated by qRT-PCR, revealing that it is a very early event in the course of reprogramming (Figure S4E). Interestingly, ISX9 was not potent in downregulating *Zfp36L1* mRNA levels (Figure 5D), further supporting our initial observation that ISX9 alone cannot instruct reprogramming of astrocytes to iNs, possibly because it failed to downregulate astrocytic genes.

Since ZFP36L1 acts by mediating degradation of its mRNA targets, we were interested in identifying ZFP36L1

mRNA targets that are upregulated in our analysis. For this purpose, we combined two publicly available ZFP36L1 iCLIP-seq data from thymocytes (Vogel et al., 2016) and B lymphocytes (Galloway et al., 2016) and ended up with 621 ZFP36L1 direct targets that are upregulated in miR-124-iNs vs. sc-miRNA astro ($\log_2(\text{fold change}) \geq 1$, FDR < 0.05), which importantly correspond to 47% of miR-124 upregulated DEGs. GO enrichment analysis revealed that many of these genes are implicated in neurogenesis, neuron projection development, synaptic transmission, axonogenesis, dendritic morphogenesis, and telencephalic development (Figure 5E). Interestingly, many of them were also found to regulate transcription and RNA processing (Figure 5E), highlighting an important regulatory role for many ZFP36L1 targets with possible impact on the reprogramming process. Among these targets we found neurogenic TFs, such as *Tox*, *Tox3*, *Rcor2*, *Cux1*, *Hes6*, *Lzts1*, and *Mlt11*, and EFs related to neurogenesis such as *Chd3*, *Chd7*, *Kmt2c*, and *Tet1* (Figure 5F). Notably, we also identified as ZFP36L1 targets the neuronal RBPs *Elavl4*, *Nova1*, and *Rbfox1* (Figure 5F). This constitutes a significant finding that suggests the repression of neuronal RBPs directly by ZFP36L1, being relieved upon miR-124-mediated ZFP36L1 downregulation.

We subsequently examined the mRNA levels of the ZFP36L1 targets identified by our analysis, *Elavl4*, *Nova1*, *Rbfox1*, *Rcor2*, and *Tox*, upon miR-124 overexpression with qRT-PCR and verified that miR-124 was potent in inducing their upregulation (Figure 5G). We also verified the increase in protein levels of the neurogenic TF, TOX, in miR-124-iNs at day 5 (Figures S4F and S4G). Notably, we observed that the combination of miR-124 with ISX9 further enhanced greatly the mRNA levels of the RBPs

Figure 5. The RNA-binding protein Zfp36L1 is a novel direct target of miR-124

(A) Venn diagram of the miR-124 targets derived from Ago-HITS-CLIP and the downregulated DEGs of miR-124 vs. sc-miRNA astro RNA-seq data ($\log_2(\text{fold change}) \leq -1$, FDR < 0.01). Identified miR-124 targets were combined with a public reference list of genes, expressed in astrocytes, resulting in a set of 130 genes.

(B) miR-124 direct binding to the 3' UTR of *Zfp36L1* and *ZFP36L1* in mouse and human species, respectively. miR-124 binds with perfect seed complementarity (7mer-m8 site) in both species.

(C) Analysis of luciferase activity in HEK293T cells upon co-transfection with sc-miRNA or miR-124 mimics along with the reporter construct pmiR-GLO containing the 3' UTR of *Zfp36L1* with the miR-124 binding site ($n = 7$ independent experiments), the 3' UTR of *Zfp36L1* with the mutated miR-124 binding site ($n = 3$), or the 3' UTR of *Zfp36L2* ($n = 6$). Normalized Firefly luciferase activity for sc-miRNA has been set to 1.

(D) qRT-PCR validation of the mRNA levels of miR-124 direct target *Zfp36L1* at day 7 ($n = 3$ independent experiments).

(E) GO analysis of biological processes for ZFP36L1 direct targets that are also significantly upregulated in miR-124-iNs vs. sc-miRNA astro. GO terms are ranked according to $\log_{10}(\text{FDR})$, and the intensity legend shows the fold enrichment of each GO term.

(F) Volcano plot comparing the $\log_2(\text{fold change})$ of TPM (transcripts per million) values in the miR-124-iNs vs. sc-miRNA astro condition vs. the $\log_{10}(\text{FDR})$ values. Significantly upregulated ($\log_2(\text{fold change}) \geq 1$, FDR < 0.05) and downregulated ($\log_2(\text{fold change}) \leq -1$, FDR < 0.05) genes are shown in green and orange, respectively. Labels of *Zfp36L1* and neuronal-specific upregulated genes that are also ZFP36L1 direct targets are portrayed.

(G) qRT-PCR validation of the mRNA levels of the ZFP36L1 targets *Elavl4*, *Nova1*, *Rbfox1*, *Rcor2*, and *Tox* at day 7 ($n = 3$ independent experiments).

* $p < 0.05$, ** $p < 0.01$, *** $p < 0.001$ vs. sc-miRNA.

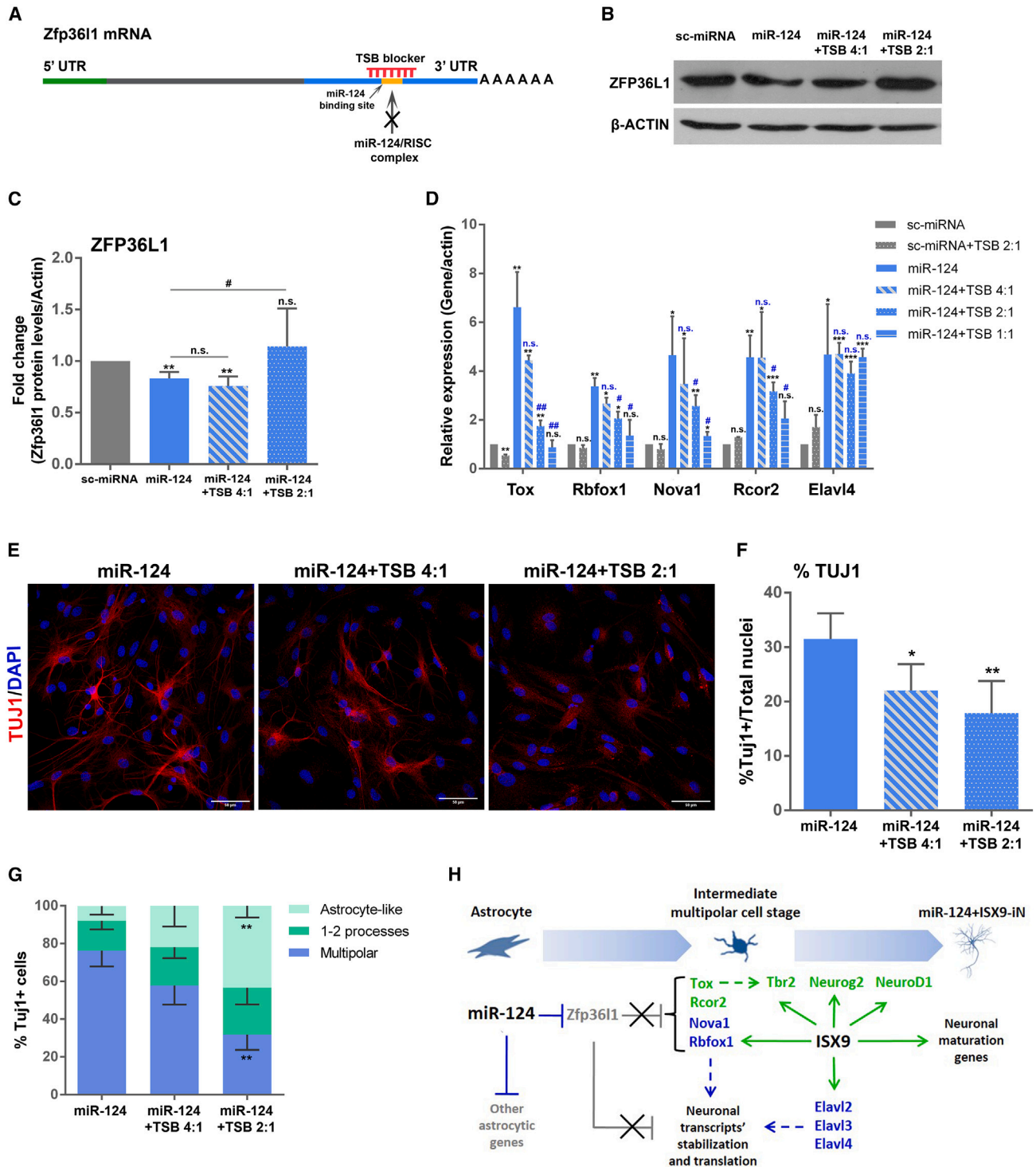


Figure 6. Targeting of Zfp361 by miR-124 plays a key role in the miR-124-induced cell fate switch of astrocytes to iNs

(A) Schematic representation of the TSB binding region in the 3' UTR of *Zfp361* mRNA.

(B) Western blot analysis of the protein levels of ZFP36L1 in the absence or presence of increasing concentrations of TSB (miR-124/TSB molecular ratio 4:1 and 2:1) at day 5 of the reprogramming protocol. Actin protein levels have been used as loading control.

(C) Quantification of ZFP36L1 protein levels normalized to β -actin. Normalized ZFP36L1 levels in sc-miRNA transfected astrocytes have been set to 1 ($n = 3$ independent experiments; ** $p < 0.01$ vs. sc-miRNA, # $p < 0.05$ vs. miR-124).

(legend continued on next page)



identified as targets of ZFP36L1, *Elavl4*, and *Rbfox1* (Figure S4H), as well as the other neuronal RBPs of the nELAVL family, *Elavl2* (Figure S4I) and *Elavl3* (Figure S4J), highlighting the importance of ISX9 in reinforcing and supplementing the neurogenic action of miR-124.

Collectively, these data show that the targets of ZFP36L1 identified here correspond to half of the miR-124-upregulated genes, and many of them constitute neuronal-specific genes with important regulatory functions. Thus, the miR-124/*Zfp36L1* interaction bears the potential to play a key regulatory role in the control of the neurogenic reprogramming switch of astrocytes by miR-124.

Targeting of *Zfp36L1* by miR-124 plays a key role in the miR-124-induced cell fate switch of astrocytes to iNs

To investigate the impact of the miR-124/*Zfp36L1* interaction on the miR-124-mediated reprogramming of astrocytes, we used a target site blocker (TSB) oligonucleotide that competitively binds to miR-124 binding site on the 3' UTR of *Zfp36L1* mRNA, blocking its downregulation by the miR-124-RISC complex (Figure 6A). The moderate downregulation of ZFP36L1 protein by miR-124 as early as day 5 of reprogramming was reversed by TSB at the miR-124/TSB molecular ratio of 2:1 (Figures 6B and 6C), while we observed no significant effect of TSB on ZFP36L2 protein levels (Figures S5A and S5B). Owing to extensive stress and cell death, it was not possible to estimate the effect of TSB on the reversal of ZFP36L1 protein levels upon miR-124 overexpression at a later time point of the reprogramming.

Next, we tested the effect of TSB on the mRNA levels of the identified neuronal targets of ZFP36L1, *Tox*, *Rbfox1*, *Nova1*, *Rcor2*, and *Elavl4* by qRT-PCR initially at day 3 and observed a dose-dependent reduction of the miR-124-induced upregulation of *Tox*, *Rbfox1*, *Nova1*, and *Rcor2*, but not of *Elavl4*, in the presence of increasing concentrations of TSB (Figure 6D). The mRNA levels of *Tox* and *Rbfox1* retained the same response to TSB at a later time

point, at day 5 (Figures S5C and S5D), an effect that was not observed for *Nova1*, *Rcor2*, and *Elavl4* (Figure S5E), implying that their post-transcriptional regulation becomes more complex as the neuronal conversion is gradually established. Importantly, TSB resulted in a significant and dose-dependent reduction in the percentage of TUJ1⁺ miR-124-iNs at day 5 (Figures 6E and 6F), with an evident alteration of their characteristic immature neuronal morphology (Figures 6E and 6G). More specifically, morphological analysis of the number of processes extending from the soma and the size of the soma of TUJ1⁺ cells indicated that TSB addition resulted in gradual abolishment of their multipolar morphology with fine processes, characteristic of miR-124-iNs (Figures 6E and 6G), and instead largely led to the retention of a premature astrocyte-like morphology with bigger soma (Figure S5F) and none or very few processes (Figures 6E and 6G). These observations strongly indicate that the targeting of *Zfp36L1* by miR-124 is an important event during the miR-124-induced reprogramming by unlocking regulatory neurogenic genes and controlling the necessary morphological changes (Figure 6H).

miR-124 induces reprogramming of resident reactive astrocytes to immature iNs *in vivo* following cortical trauma

To evaluate the *in vivo* reprogramming potential of miR-124 to drive fate conversion of resident reactive cortical astrocytes to iNs alone or in synergy with ISX9, we applied two viral-based approaches (using lentiviral [LV] and adeno-associated viral [AAV] vectors) to overexpress miR-124 into the mechanically injured cortex of 3-month-old mice. Initially, we stereotactically injected either control LV-GFP or LV-miR-124-GFP to transduce reactive astrocytes surrounding the cortical injury site, while ISX9 was systematically administered for 5 consecutive days beginning 2 days post viral injection (p.i.) in a group of mice (Figure 7A). Seven days p.i. the majority of transduced cells

(D) qRT-PCR analysis of the mRNA levels of the ZFP36L1 targets *Tox*, *Rbfox1*, *Nova1*, *Rcor2*, and *Elavl4* in the presence or absence of increasing concentrations of TSB (miR-124/TSB 4:1, 2:1, and 1:1) at day 3 (n = 3 independent experiments; *p < 0.05, **p < 0.01, ***p < 0.001 vs. sc-miRNA; #p < 0.05, ##p < 0.01 vs. miR-124).

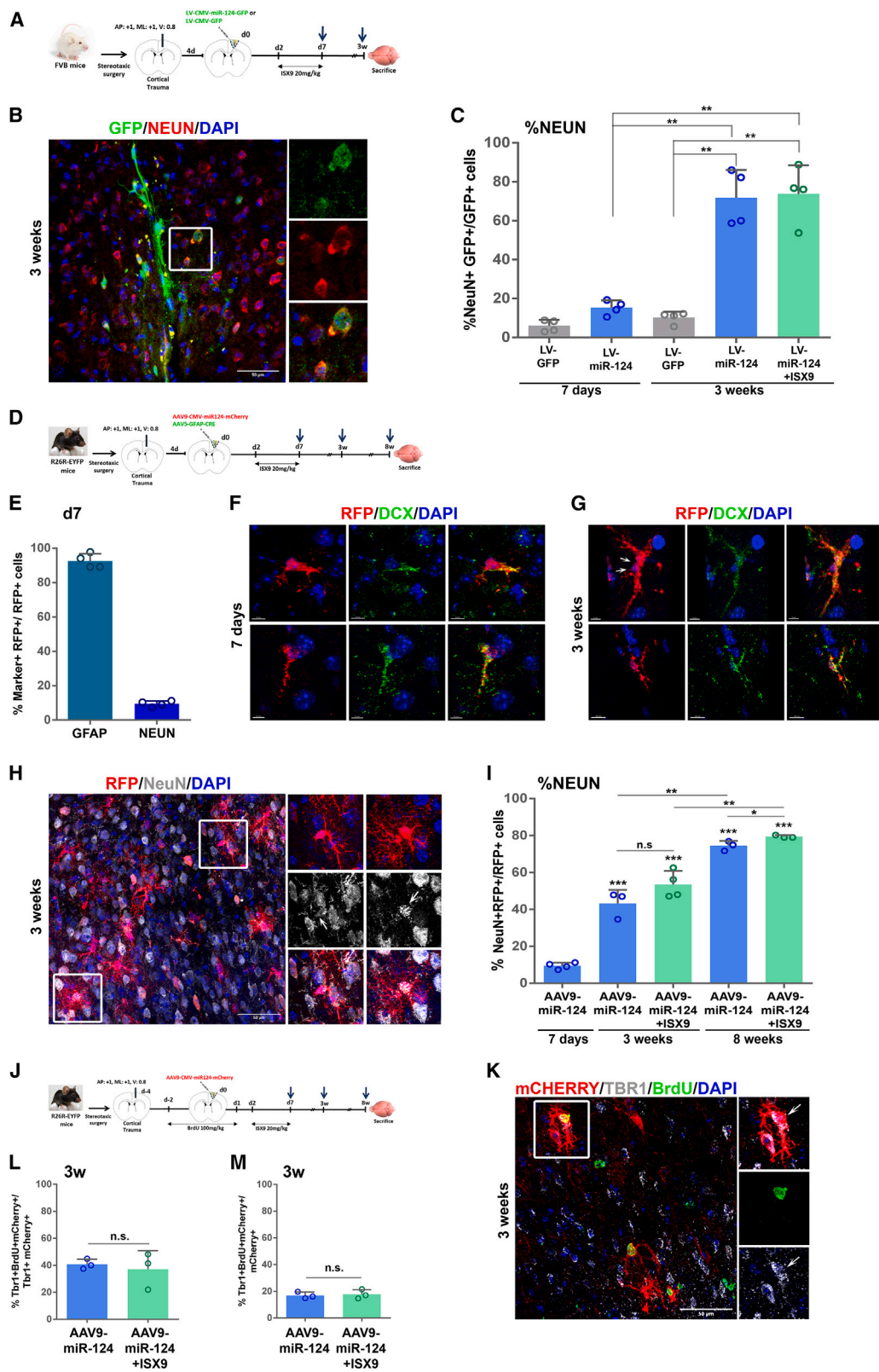
(E) Immunostaining of astrocytes reprogrammed with miR-124 or miR-124 along with increasing concentrations of TSB (4:1 and 2:1) with anti-TUJ1 antibody at day 5.

(F) Quantification of the percentage of TUJ1⁺ cells at day 5 (n = 3 independent experiments; *p < 0.05, **p < 0.01 vs. miR-124).

(G) Morphological characterization of TUJ1⁺ cells at day 5. Quantification of the percentages of multipolar TUJ1⁺ cells (3 or more processes), TUJ1⁺ cells with 1–2 processes, and TUJ1⁺ cells with an astrocyte-like morphology (rectangular soma with none or 1–2 processes) (n = 3 independent experiments; **p < 0.01 vs. miR-124).

(H) Proposed model of independent and cooperative transcriptional and post-transcriptional contributions of miR-124 and ISX9 in miR-124/ISX9-induced direct neuronal conversion of cortical astrocytes. Post-transcriptional events and RBPs are highlighted in blue, transcriptional events along with TFs in green, and downregulated genes and (blocked) inhibitory mechanisms in gray (dashed lines present knowledge from the literature).

Scale bars, 50 μ m.



(legend on next page)



surrounding the injury site (Figure S6A) in both conditions were GFAP⁺ reactive astrocytes (71.6% in LV-GFP and 65.7% in LV-miR-124-GFP), while NeuN⁺ neurons were much fewer (6.4% in LV-GFP and 15.3% in LV-miR-124-GFP) (Figure S6B). Three weeks p.i. 71.8% of the LV-miR-124 cells were NeuN⁺ while only 10.2% of the LV-GFP cells were NeuN⁺, exhibiting no significant difference between 7 days and 3 weeks (Figures 7B and 7C). Interestingly, few LV-miR-124-transduced cells at 3 weeks p.i. expressed the immature neurons' marker doublecortin (DCX) (Figure S6C). These results point to a strong potential of miR-124 to drive direct conversion of reactive astrocytes into iNs *in vivo*, while the administration of ISX9 showed no further significant contribution to this conversion (Figure 7C). The vast majority of NeuN⁺ iNs in both groups were also positive for the cortical marker TBR1 (Figures S6D and S6E).

To further validate the astrocytic origin of iNs upon miR-124 overexpression in the same cortical trauma model, we also employed a viral lineage-tracing strategy by stereotactically co-injecting AAV5-GFAP-Cre virus to mark cortical astrocytes, along with AAV9-CMV-miR-124-mCherry virus to overexpress miR-124 in the cells of the injured cortex of R26R-EYFP reporter mice (Figure 7D). However, we observed unexpected GFP expression in peritraumatic resident neurons besides its expression in astrocytes as early as 7 days after AAV5-GFAP-Cre injection (Figure S6F), indicating that in accordance with recent reports (Wang et al., 2021) this approach cannot warrant exclusive astrocytic lineage tracing. Given this limitation, we restricted our analysis to the AAV9-CMV-miR-124-transduced cells, also employing BrdU to label the proliferating astrocytes of the peritraumatic area. The majority of miR-124-transduced cells 7 days p.i. were GFAP⁺ reactive astrocytes (92.5%) with only 9.5% being NeuN⁺ neurons (Figures 7E

and S6G), while few MASH1⁺/RFP⁺ cells were also present (Figure S6H). Notably, 42.3% of miR-124-transduced cells 7 days p.i. and 26% 3 weeks p.i. were DCX⁺ immature iNs (Figures 7F, 7G, and S6I), while 42.8% of miR-124-transduced cells 3 weeks p.i. exhibited NeuN positivity while still retaining an immature neuronal morphology (Figures 7H and 7I). ISX9 administration along with miR-124 led to a small decrease in DCX⁺/RFP⁺ cells (18.8%) (Figure S6I) along with a non-significant increase in NeuN⁺/RFP⁺ cells (51.6%) (Figure 7I) without conferring further morphological maturation, although a 30% statistically significant increase in *NeuroD1* mRNA levels was detected in the lesioned cortex of animals receiving ISX9 (Figure S6J). Similar to the lentiviral approach, in both conditions iNs also expressed TBR1 (41.2% in miR-124 and 51.4% in miR-124 + ISX9) (Figure S6K) at the same percentages with NeuN.

Further analysis at 8 weeks p.i. revealed that the percentage of NeuN⁺ iNs increased to 74.5%, with a small but statistically significant additional increase (79.4%) in the miR-124 + ISX9 group (Figure 7I). The average number of remaining NeuN⁺ iNs per section was 30%–50% lower at 8 weeks p.i. compared with 3 weeks p.i. in both conditions (Figure S6L). Importantly, the average number of NeuN⁺ iNs in the miR-124 + ISX9 group was almost double that of the miR-124 group (Figure S6L), indicating that ISX9 enhances iNs survival. We also detected a small number of RFP⁺ cells in both groups that were VGlut2⁺ (Figure S7A), or exhibited parvalbumin (PV)⁺ puncta (Figure S7B), being at close proximity with GABA α receptor scaffold protein gephyrin (GPHN)⁺ puncta (Figures S7C and S7D); however, in both conditions iNs retained an immature morphology (Figures S6M and S7J).

Of note, mCherry expression was also observed in several resident pyramidal neurons, mostly in the broader

Figure 7. miR-124 induces reprogramming of resident reactive astrocytes to iNs with cortical identity *in vivo* following cortical trauma

- (A) Experimental setup for the lentiviral approach.
 - (B) LV-124-transduced cells in the peritraumatic cortical parenchyma expressing NeuN 3 weeks p.i. Scale bars, 50 μ m.
 - (C) Percentage of control LV-GFP and LV-124-transduced cells expressing NeuN 7 days and 3 weeks p.i. \pm ISX9 (n = 4 animals per group per time point).
 - (D) Experimental setup for the AAV approach.
 - (E) Percentage of AAV9-124-transduced cells in the peritraumatic area expressing GFAP or NeuN 7 days p.i. (n = 4 animals).
 - (F and G) Representative AAV9-124-transduced cells (in red detected with an anti-RFP antibody) expressing DCX 7 days p.i. (scale bars, 8 and 5 μ m, respectively) (F) and 3 weeks p.i. (scale bars, 5 and 10 μ m, respectively) (G).
 - (H) AAV9-124-transduced cells expressing NeuN 3 weeks p.i. Scale bars, 50 μ m.
 - (I) Percentage of AAV9-miR-124-transduced cells expressing NeuN 7 days, 3 weeks, and 8 weeks p.i. \pm ISX9 (n = 3–4 animals per group per time point).
 - (J) Experimental setup for the BrdU administration.
 - (K) miR-124 cells (in red detected with an anti-mCherry antibody) express TBR1 and have incorporated BrdU 3 weeks p.i. Scale bars, 50 μ m.
 - (L and M) Percentage of TBR1⁺/mCherry⁺ cells that originated from a proliferating state (BrdU⁺) (L) and percentage of mCherry⁺ cells that originated from a proliferating state and have undergone reprogramming (TBR1⁺/BrdU⁺) 3 weeks p.i. (M) (n = 3 animals per group).
- *p < 0.05, **p < 0.01, ***p < 0.001.



peritraumatic region at both time points, a phenomenon recently pointed out for AAVs (Wang et al., 2021); however, mCherry⁺ resident pyramidal neurons were excluded from our analysis as they were easily distinguished by their morphology (large conic soma and large apical process) (Figures S7E and S7F).

To validate that produced iNs are the result of a reprogramming process, we next administered BrdU for 4 consecutive days starting 2 days p.i. to label proliferating reactive astrocytes of the peritraumatic area (Figure 7J). Nearly one-third of transduced astrocytes (29.5%) 7 days p.i. had incorporated BrdU (Figure S7G), while BrdU⁺ transduced cells were still present 3 weeks p.i. in both conditions (34.5% for miR-124 and 33.5% for miR-124 + ISX9) (Figure S7H). Importantly, 3-week p.i. iNs originating from a proliferating state expressing TBR1 (Figures 7K and S7I) and NeuN (Figure S7K) were present. More specifically, 40.8% of miR-124-TBR1⁺ cells and 37.2% of miR-124 + ISX9-TBR1⁺ cells were BrdU⁺ (Figure 7L), accounting to nearly one-fifth of all transduced cells (Figure 7M). Of note, BrdU⁺/TBR1⁺ iNs were still present at 8 weeks p.i. (Figures S7J and S7L).

These findings collectively indicate that a significant subpopulation of iNs originates from a proliferating fraction of reactive astrocytes. They also show that miR-124 is sufficient to drive on its own neurogenic reprogramming of reactive astrocytes to immature iNs that remain viable within the injured cortex for a period of at least 8 weeks, while ISX9 contributes to enhancement of iNs survival.

DISCUSSION

In this study, we attempted to isolate the mechanism of action of miR-124 from that of other reprogramming co-factors and provide evidence that miR-124 drives the *trans*-differentiation switch of cortical astrocytes to an immature iN phenotype of cortical identity by downregulating astrocytic genes with regulatory function and directing astrocytes through a multipolar intermediate stage expressing genes related to the transcriptional signature of endogenous IPCs (Ruan et al., 2021). To enhance iNs' maturation, we supplemented miR-124 with the neurogenic compound ISX9, which is known to upregulate neuronal-specific genes including *NeuroD1* (Schneider et al., 2008) and has already been used in chemical reprogramming protocols (Gao et al., 2017; Li et al., 2015). Indeed, ISX9 greatly improved iNs' differentiation status, leading to the acquisition of electrophysiologically active iNs. Interestingly, despite upregulation of *NeuroD1* and many other neuronal TFs by ISX9 alone, control sc-miRNA + ISX9-treated astrocytes failed to undergo reprogramming, most probably due to the fact that high levels of *NeuroD1*—not triggered by ISX9 supplementation in

our system—are required to exert its neuronal reprogramming capacity (Matsuda et al., 2019; Pataskar et al., 2016).

Analysis of the direct miR-124 targets by combining our RNA-seq data with Ago HITS-CLIP data from mouse (Chi et al., 2009) and human cortex (Boudreau et al., 2014) revealed the RBP *Zfp36L1* as a novel target of miR-124, being conserved during mammalian brain evolution. Many studies have identified several direct targets of miR-124 with important regulatory roles in neurogenesis, acting at the transcriptional level, such as the TFs *Sox9* (Cheng et al., 2009) and *Lhx2* (Sanuki et al., 2011) and REST complex components *Scp1* (Visvanathan et al., 2007) and *Rcor1* (Baudet et al., 2012), or at the epigenetic level, such as *Ezh2* and *BAF53a* (Neo et al., 2014) as well as at the post-transcriptional level, such as the alternative splicing RBP *Pthp1* (Makeyev et al., 2007).

Here, we report for the first time that miR-124 is directly implicated in the regulation of another process mediated by RBPs, mRNA decay, apart from the well-characterized miR-124/*Pthp1* circuitry (Yeom et al., 2018). ZFP36L1 is a member of the ZFP36 family along with ZFP36 and ZFP36L2, which mediate the destabilization of their mRNA targets through binding to AU-rich elements (AREs) in their 3' UTRs (Lai et al., 2000) and are expressed in radial glia and cortical glial cells (Weng et al., 2019). ARE-mediated mRNA decay is also regulated by miR-9, which targets the close paralog of ZFP36L1, *Zfp36* (Dai et al., 2015), suggesting a combined regulation of ZFP36 family members by these neurogenic miRNAs to increase the stabilization of neuronal mRNAs during neurogenesis.

Furthermore, examination of data from ZFP36L1-iCLIP-seq experiments (Galloway et al., 2016; Vogel et al., 2016) revealed several ZFP36L1 downstream targets regulated in miR-124-iNs with a significant regulatory role in neurogenesis, such as the TFs *Tox* and *Rcor2* and the RBPs *Rbfox1*, *Elavl4*, and *Nova1*. Importantly, disruption of miR-124/*Zfp36L1* interaction negatively impacted the reprogramming process, reducing the number of TUJ1⁺ miR-124-iNs and abolishing their multipolar morphology. Of note, based on this approach, *Rbfox1* and *Nova1* exhibited a pattern of direct post-transcriptional regulation by ZFP36L1 in contrast to *Elavl4*, implying a stronger involvement of other RBPs in its post-transcriptional regulation. In accordance with this, ZFP36 has been reported to target *Elavl2*, *Elavl3*, *Elavl4*, and *Nova1* (Dai et al., 2015), uncovering a complementary and synergistic role of ZFP36L1 and ZFP36 in repressing neuron-specific RBPs in non-neuronal cells.

The addition of ISX9 significantly contributed to the robust upregulation of *Rbfox1*, *Elavl2*, *Elavl4*, and most prominently *Elavl3*, reinforcing the action of miR-124 in inducing the switch from the neuronal transcripts' destabilizing RBPs to the stabilizing neuronal RBPs (Weyn-Vanhentenryck



et al., 2014; Scheckel et al., 2016) through a different mechanism that needs further exploration. Interestingly, miR-124 has been recently shown to synergize with ELAVL3 for the enhancement of target genes' expression during neuronal differentiation (Lu et al., 2021), supporting our observations on the cooperative action of miR-124/ISX9 in promoting iNs' maturation (Figure 6H).

Here we also explored the *in vivo* capacity of miR-124 to induce direct neurogenic reprogramming of astrocytes in a mouse cortical injury model, known to render astrocytes more plastic and prone to reprogramming by activating NSC genes' expression (Götz et al., 2015). *In vivo* reprogramming of reactive astrocytes to neuronal precursors and iNs has been achieved following forced expression of TF/miRNA cocktails (Rivetti Di Val Cervo et al., 2017; Matugini et al., 2019; Qian et al., 2020; Lentini et al., 2021; Drouin-Ouellet et al., 2022), in some cases combined with antiapoptotic/antioxidant treatment to enhance survival (Gascón et al., 2016). However, the *in vivo* neurogenic capacity of miR-124 on its own has not been evaluated up to now. In the last years, the functional restoration of disease-related symptoms upon direct reprogramming has been reported (Giehl-Schwab et al., 2022; Qian et al., 2020; Zhou et al., 2020; Wu et al., 2020; Chen et al., 2019), supporting the therapeutic promise of *in vivo* direct reprogramming to restore impaired neuronal circuits (Bocchi et al., 2022). However, certain AAV-based strategies and astrocyte-lineage-tracing approaches have been very recently put under question for their capacity to confer neurogenic reprogramming (Wang et al., 2021). In view of this new challenge in the *in vivo* reprogramming field, we employed two different viral-based approaches using either lentiviruses or AAVs and provide substantial evidence indicating the capacity of miR-124 to convert cortical peritraumatic reactive astrocytes to immature iNs expressing TBR1 and NeuN postmitotic neuronal markers. Importantly, our AAV-based protocol combined with BrdU—one of the few widely accepted tools currently available—to verify the non-neuronal origin of reprogrammed cells showed that about one-third of iNs originate from proliferating astrocytes. This finding along with the presence of DCX⁺ miR-124-transduced cells strongly supports the non-neuronal origin of produced iNs. Interestingly at 8 weeks p.i., in accordance with our *in vitro* observations, few iNs acquired glutamatergic identity expressing VGlut2 and exhibited PV⁺/GPHN⁺ puncta at close proximity that are indicative of synapse formation initiation with inhibitory neurons.

These findings indicate that, similarly to the *in vitro* situation, miR-124 is capable of inducing the reprogramming switch of peritraumatic reactive astrocytes but is not sufficient to further enhance maturation of produced iNs. *In vivo* administration of ISX9 acts beneficially to

reprogramming by contributing majorly to iNs' enhanced survival for a longer period, but in contrast to our *in vitro* observations it does not seem to reinforce iNs maturation, although it is potent in moderately upregulating NeuroD1 levels, proving that it crosses the blood-brain barrier in the scheme administered by us (Bettio et al., 2016). In the light of recent developments on the field of glia-to-neuron conversion regarding viral approaches (Wang et al., 2021), a limitation of our current *in vivo* approach is the absence of a genetic lineage-tracing model—verifying iNs' astrocytic origin—which, combined with scRNA-seq, would give robust confirmation of the *in vivo* reprogramming processes and uncover transcriptional states of iNs.

Taken together, this study highlights the strong potency of miR-124 to instruct the cell fate switch of astrocytes, post-transcriptionally triggering cortical neurogenesis pathways being unlocked in part by the direct targeting of *Zfp36L1*. Importantly, our findings point toward the *in vivo* capacity of miR-124 to induce reactive astrocytes' reprogramming to immature iNs that are able to survive for long periods, particularly following ISX9 supplementation. However, miR-124/ISX9 synergistic action does not seem to be sufficient to drive iNs' full maturation, indicating that more intrinsic and/or extrinsic cues are required. To this end, certain transcriptional and post-transcriptional downstream effectors of miR-124 and ISX9 identified here bear the potential to amplify miR-124/ISX9 combined *in vivo* reprogramming action and enhance iNs' maturation. This strategy is in accordance with the view that *in vivo* glia-to-neuron conversion is a two-stage process involving initial immature iNs production and their subsequent differentiation provided that certain still unknown barriers are overcome (Leaman et al., 2022). Thus, focusing on the points of convergence of miR-124/ISX9 action holds promise for the establishment of a more efficient, *in vivo* reprogramming protocol to improve functional maturation of iNs following trauma or neurodegeneration.

EXPERIMENTAL PROCEDURES

Resource availability

Corresponding author

Further information and requests for resources and reagents should be directed to the corresponding author, Dimitra Thomaidou (thomaidou@pasteur.gr).

Materials availability

The constructs created for this study can be requested from the corresponding author.

Data availability

RNA-seq data are deposited in the European Nucleotide Archive under study accession ENA: PRJEB38603.



***In vitro* astrocytic reprogramming**

Astrocytes were *in vitro* reprogrammed to iNs, following triple transfection with 80 nM miR-124-3p mimics or sc-miRNA mimics (Thermo) using Lipofectamine 2000 (Invitrogen). For the functional validation of miR-124/Zfp36L1 interaction, a custom-made miRCURY LNA miRNA Power TSB (Qiagen) was transfected into astrocytes along with sc-miRNA or miR-124-3p mimics.

Analysis of Ago HITS-CLIP data

Ago HITS-CLIP datasets, performed in mouse brain cortex tissue (P13 neocortex) and human brain tissues (motor cortex, cingulate gyrus) from two individuals retrieved from published data were aligned against the reference genomes, with GMAP/GSNAP spliced aligner, allowing up to two mismatches. The microCLIP CLIP-seq-guided model was utilized to identify binding events for the expressed miRNAs. Human and mouse transcriptomes were compiled from ENSEMBL v96 to annotate the retrieve miRNA binding events. Identified miRNA binding sites residing on 3' UTR regions were retained and subsequently filtered to preserve only genes expressed in astrocytes.

***In vivo* astrocytic reprogramming**

For *in vivo* miR-124 administration, 4 days following cortical trauma either VSV-G–pseudotyped lentivirus expressing miR-124-GFP or AAV9 expressing miR-124-mCherry were stereotactically injected into the cortex at coordinates (AP) –1.1 mm, (L) 1.0 mm, and (V) 1.0 mm. Subgroups of LV-124-GFP or AAV-9-miR-124-mCherry-transduced mice received intraperitoneally 20 mg/kg ISX9 (Tocris), for 5 days, beginning 48 h p.i. Mice were sacrificed 1, 3, and 8 weeks p.i.

Extended experimental procedures are described in [supplemental information](#).

SUPPLEMENTAL INFORMATION

Supplemental information can be found online at <https://doi.org/10.1016/j.stemcr.2023.02.009>.

AUTHOR CONTRIBUTIONS

E.P. and D.T. conceived project, designed experiments, and analyzed data; E.P., C.G., M.G., and M.M. conducted *in vitro* experiments; D.C.-T. and S.J.T. designed and performed electrophysiology experiments; D.K., T.K., and A.G.H. designed and performed bioinformatics analysis, and E.P. contributed to analyzing the data; P.N.K. and I.T. designed and performed *in vivo* experiments, and P.N.K. and E.P. analyzed relevant *in vivo* data; E.X. developed the Fiji macro and helped with image analysis; E.P. and D.T. wrote the manuscript; D.T. supervised the project and acquired funding.

ACKNOWLEDGMENTS

This work was financially supported by “BIOIMAGING-GR (MIS 5002755)”, co-financed by Greece and EU Regional Development Fund, ARISTEIA-II “Astro-Rep” 3713 grant of the Greek Ministry

of Education and Fondation Santé grant 2017–2018, awarded to D.T. We also acknowledge funding from Stavros Niarchos Foundation to Hellenic Pasteur Institute, as part of the Foundation’s initiative to support the Greek Research Center Ecosystem; Greek “Flagship Action for the Study of Neurodegenerative Diseases on the Basis of Precision Medicine” and “KRIPIS-II” Action (MIS 5002486). We would like to thank Dr. Era Taoufik for critical comments on the manuscript.

CONFLICT OF INTERESTS

The authors declare no competing interests.

Received: June 14, 2022

Revised: February 21, 2023

Accepted: February 23, 2023

Published: March 23, 2023

REFERENCES

- Abernathy, D.G., Kim, W.K., McCoy, M.J., Lake, A.M., Ouwenga, R., Lee, S.W., Xing, X., Li, D., Lee, H.J., Heuckeroth, R.O., et al. (2017). MicroRNAs induce a permissive chromatin environment that enables neuronal subtype-specific reprogramming of adult human fibroblasts. *Cell Stem Cell* 21, 332–348.e9. <https://doi.org/10.1016/j.stem.2017.08.002>.
- Acaz-Fonseca, E., Ortiz-Rodriguez, A., Azcoitia, I., Garcia-Segura, L.M., and Arevalo, M.A. (2019). Notch signaling in astrocytes mediates their morphological response to an inflammatory challenge. *Cell Death Dis.* 5, 85. <https://doi.org/10.1038/s41420-019-0166-6>.
- Aravantinou-Fatorou, K., Ortega, F., Chroni-Tzartou, D., Antoniou, N., Pouloupoulou, C., Politis, P.K., Berninger, B., Matsas, R., and Thomaidou, D. (2015). CEND1 and NEUROGENIN2 reprogram mouse astrocytes and embryonic fibroblasts to induced neural precursors and differentiated neurons. *Stem Cell Rep.* 5, 405–418. <https://doi.org/10.1016/j.stemcr.2015.07.012>.
- Baudet, M.L., Zivraj, K.H., Abreu-Goodger, C., Muldal, A., Armisen, J., Blenkiron, C., Goldstein, L.D., Miska, E.A., and Holt, C.E. (2012). MiR-124 acts through CoREST to control onset of Sema3A sensitivity in navigating retinal growth cones. *Nat. Neurosci.* 15, 29–38. <https://doi.org/10.1038/nn.2979>.
- Bettio, L.E.B., Patten, A.R., Gil-Mohapel, J., O'Rourke, N.F., Hanley, R.P., Kennedy, S., Gopalakrishnan, K., Rodrigues, A.L.S., Wulff, J., and Christie, B.R. (2016). ISX-9 can potentiate cell proliferation and neuronal commitment in the rat dentate gyrus. *Neuroscience* 332, 212–222. <https://doi.org/10.1016/j.neuroscience.2016.06.042>.
- Birtele, M., Sharma, Y., Kidnapillai, S., Lau, S., Stoker, T.B., Barker, R.A., Rylander Ottosson, D., Drouin-Ouellet, J., and Parmar, M. (2019). Dual modulation of neuron-specific microRNAs and the REST complex promotes functional maturation of human adult induced neurons. *FEBS Lett.* 593, 3370–3380. <https://doi.org/10.1002/1873-3468.13612>.
- Bocchi, R., Masserdotti, G., and Götz, M. (2022). Direct neuronal reprogramming: fast forward from new concepts toward therapeutic approaches. *Neuron* 110, 366–393. <https://doi.org/10.1016/j.neuron.2021.11.023>.



- Boudreau, R.L., Jiang, P., Gilmore, B.L., Spengler, R.M., Tirabassi, R., Nelson, J.A., Ross, C.A., Xing, Y., and Davidson, B.L. (2014). Transcriptome-wide discovery of microRNA binding sites in Human Brain. *Neuron* 81, 294–305. <https://doi.org/10.1016/j.neuron.2013.10.062>.
- Carrick, D.M., and Blackshear, P.J. (2007). Comparative expression of tristetraprolin (TTP) family member transcripts in normal human tissues and cancer cell lines. *Arch. Biochem. Biophys.* 462, 278–285. <https://doi.org/10.1016/j.abb.2007.04.011>.
- Chen, Y.C., Ma, N.X., Pei, Z.F., Wu, Z., Do-Monte, F.H., Keefe, S., Yellin, E., Chen, M.S., Yin, J.C., Lee, G., et al. (2019). A NeuroD1 AAV-based gene therapy for functional brain repair after ischemic injury through in vivo astrocyte-to-neuron conversion. *Mol. Ther.* 28, 217–234. <https://doi.org/10.1016/j.ymthe.2019.09.003>.
- Cheng, L.C., Pastrana, E., Tavazoie, M., and Doetsch, F. (2009). MiR-124 regulates adult neurogenesis in the subventricular zone stem cell niche. *Nat. Neurosci.* 12, 399–408. <https://doi.org/10.1038/nn.2294>.
- Chi, S.W., Zang, J.B., Mele, A., and Darnell, R.B. (2009). Argonaute HITS-CLIP decodes microRNA-mRNA interaction maps. *Nature* 460, 479–486. <https://doi.org/10.1038/nature08170>.
- Dai, W., Li, W., Hoque, M., Li, Z., Tian, B., and Makeyev, E.V. (2015). A post-transcriptional mechanism pacing expression of neural genes with precursor cell differentiation status. *Nat. Commun.* 6, 7576. <https://doi.org/10.1038/ncomms8576>.
- Drouin-Ouellet, J., Legault, E.M., Nilsson, F., Piracs, K., Bouquety, J., Petit, F., Shrigley, S., Birtele, M., Pereira, M., Storm, P., et al. (2022). Age-related pathological impairments in directly reprogrammed dopaminergic neurons derived from patients with idiopathic Parkinson's disease. *Stem Cell Rep.* 17, 2203–2219. <https://doi.org/10.1016/j.stemcr.2022.08.010>.
- Elsen, G.E., Bedogni, F., Hodge, R.D., Bammler, T.K., MacDonald, J.W., Lindtner, S., Rubenstein, J.L.R., and Hevner, R.F. (2018). The epigenetic factor landscape of developing neocortex is regulated by transcription factors Pax6 → Tbr2 → Tbr1. *Front. Neurosci.* 12, 571. <https://doi.org/10.3389/fnins.2018.00571>.
- Galloway, A., Saveliev, A., Łukasiak, S., Hodson, D.J., Bolland, D., Balmano, K., Ahlfors, H., Monzón-Casanova, E., Mannurita, S.C., Bell, L.S., et al. (2016). RNA-binding proteins ZFP36L1 and ZFP36L2 promote cell quiescence. *Science* 352, 453–459. <https://doi.org/10.1126/science.aad5978>.
- Gao, L., Guan, W., Wang, M., Wang, H., Yu, J., Liu, Q., Qiu, B., Yu, Y., Ping, Y., Bian, X., et al. (2017). Direct generation of human neuronal cells from adult astrocytes by small molecules. *Stem Cell Rep.* 8, 538–547. <https://doi.org/10.1016/j.stemcr.2017.01.014>.
- Gascón, S., Murenu, E., Masserdotti, G., Ortega, F., Russo, G.L., Petrik, D., Deshpande, A., Heinrich, C., Karow, M., Robertson, S.P., et al. (2016). Identification and successful negotiation of a metabolic checkpoint in direct neuronal reprogramming. *Cell Stem Cell* 18, 396–409. <https://doi.org/10.1016/j.stem.2015.12.003>.
- Giehl-Schwab, J., Giesert, F., Rauser, B., Lao, C.L., Hembach, S., Lefort, S., Ibarra, I.L., Koupourtidou, C., Lueken, M.D., Truong, D.J.J., et al. (2022). Parkinson's disease motor symptoms rescue by CRISPRa-reprogramming astrocytes into GABAergic neurons. *EMBO Mol. Med.* 14, 147977–e14820. <https://doi.org/10.15252/emmm.202114797>.
- Götz, M., Sirko, S., Beckers, J., and Irmeler, M. (2015). Reactive astrocytes as neural stem or progenitor cells: in vivo lineage, in vitro potential, and Genome-wide expression analysis. *Glia* 63, 1452–1468. <https://doi.org/10.1002/glia.22850>.
- Guo, Z., Zhang, L., Wu, Z., Chen, Y., Wang, F., and Chen, G. (2014). In vivo direct reprogramming of reactive glial cells into functional neurons after brain injury and in an Alzheimer's disease model. *Cell Stem Cell* 14, 188–202. <https://doi.org/10.1016/j.stem.2013.12.001>.
- Heinrich, C., Blum, R., Gascón, S., Masserdotti, G., Tripathi, P., Sánchez, R., Tiedt, S., Schroeder, T., Götz, M., and Berninger, B. (2010). Directing astroglia from the cerebral cortex into subtype specific functional neurons. *PLoS Biol.* 8, e1000373. <https://doi.org/10.1371/journal.pbio.1000373>.
- Hong, C.J., and Hsueh, Y.P. (2007). Cytoplasmic distribution of T-box transcription factor Tbr-1 in adult rodent brain. *J. Chem. Neuroanat.* 33, 124–130. <https://doi.org/10.1016/j.jchemneu.2007.01.005>.
- Lai, W.S., Carballo, E., Thorn, J.M., Kennington, E.A., and Blackshear, P.J. (2000). Interactions of CCCH zinc finger proteins with mRNA. Binding of tristetraprolin-related zinc finger proteins to AU-rich elements and destabilization of mRNA. *J. Biol. Chem.* 275, 17827–17837. <https://doi.org/10.1074/jbc.M001696200>.
- Leaman, S., Marichal, N., and Berninger, B. (2022). Reprogramming cellular identity in vivo. *Development* 149, dev200433. <https://doi.org/10.1242/dev.200433>.
- Lentini, C., d'Orange, M., Marichal, N., Trottmann, M.M., Vignoles, R., Foucault, L., Verrier, C., Massera, C., Raineteau, O., Conzelmann, K.K., et al. (2021). Reprogramming reactive glia into interneurons reduces chronic seizure activity in a mouse model of mesial temporal lobe epilepsy. *Cell Stem Cell* 28, 2104–2121.e10. <https://doi.org/10.1016/j.stem.2021.09.002>.
- Li, X., Zuo, X., Jing, J., Ma, Y., Wang, J., Liu, D., Zhu, J., Du, X., Xiong, L., Du, Y., et al. (2015). Small-molecule-driven direct reprogramming of mouse fibroblasts into functional neurons. *Cell Stem Cell* 17, 195–203. <https://doi.org/10.1016/j.stem.2015.06.003>.
- Lu, Y.L., Liu, Y., McCoy, M.J., and Yoo, A.S. (2021). MiR-124 synergism with ELAVL3 enhances target gene expression to promote neuronal maturity. *Proc. Natl. Acad. Sci. USA* 118, e2015454118. <https://doi.org/10.1073/pnas.2015454118>.
- Luján, R., Shigemoto, R., and López-Bendito, G. (2005). Glutamate and GABA receptor signalling in the developing brain. *Neuroscience* 130, 567–580. <https://doi.org/10.1016/j.neuroscience.2004.09.042>.
- Makeyev, E.V., Zhang, J., Carrasco, M.A., and Maniatis, T. (2007). The MicroRNA miR-124 promotes neuronal differentiation by triggering brain-specific alternative pre-mRNA splicing. *Mol. Cell* 27, 435–448. <https://doi.org/10.1016/j.molcel.2007.07.015>.
- Matsuda, T., Irie, T., Katsurabayashi, S., Hayashi, Y., Nagai, T., Hamazaki, N., Adefuin, A.M.D., Miura, F., Ito, T., Kimura, H., et al. (2019). Pioneer factor NeuroD1 rearranges transcriptional and epigenetic profiles to execute microglia-neuron conversion.



- Neuron 101, 472–485.e7. <https://doi.org/10.1016/j.neuron.2018.12.010>.
- Mattugini, N., Bocchi, R., Scheuss, V., Russo, G.L., Torper, O., Lao, C.L., and Götz, M. (2019). Inducing different neuronal subtypes from astrocytes in the injured mouse cerebral cortex. *Neuron* 103, 1086–1095.e5. <https://doi.org/10.1016/j.neuron.2019.08.009>.
- Neo, W.H., Yap, K., Lee, S.H., Looi, L.S., Khandelia, P., Neo, S.X., Makeyev, E.V., and Su, I.H. (2014). MicroRNA miR-124 controls the choice between neuronal and astrocyte differentiation by fine-tuning Ezh2 expression. *J. Biol. Chem.* 289, 20788–20801. <https://doi.org/10.1074/jbc.M113.525493>.
- Pataskar, A., Jung, J., Smialowski, P., Noack, F., Calegari, F., Straub, T., and Tiwari, V.K. (2016). NeuroD1 reprograms chromatin and transcription factor landscapes to induce the neuronal program. *EMBO J.* 35, 24–45. <https://doi.org/10.15252/embj.201591206>.
- Qian, H., Kang, X., Hu, J., Zhang, D., Liang, Z., Meng, F., Zhang, X., Xue, Y., Maimon, R., Dowdy, S.F., et al. (2020). Reversing a model of Parkinson's disease with in situ converted nigral neurons. *Nature* 582, 550–556. <https://doi.org/10.1038/s41586-020-2388-4>.
- Rivetti Di Val Cervo, P., Romanov, R.A., Spigolon, G., Masini, D., Martín-Montañez, E., Toledo, E.M., La Manno, G., Feyder, M., Pifl, C., Ng, Y.H., et al. (2017). Induction of functional dopamine neurons from human astrocytes in vitro and mouse astrocytes in a Parkinson's disease model. *Nat. Biotechnol.* 35, 444–452. <https://doi.org/10.1038/nbt.3835>.
- Ruan, X., Kang, B., Qi, C., Lin, W., Wang, J., and Zhang, X. (2021). Progenitor cell diversity in the developing mouse neocortex. *Proc. Natl. Acad. Sci. USA* 118, e2018866118. <https://doi.org/10.1073/pnas.2018866118>.
- Sanuki, R., Onishi, A., Koike, C., Muramatsu, R., Watanabe, S., Muranishi, Y., Irie, S., Uneo, S., Koyasu, T., Matsui, R., et al. (2011). MiR-124a is required for hippocampal axogenesis and retinal cone survival through Lhx2 suppression. *Nat. Neurosci.* 14, 1125–1134. <https://doi.org/10.1038/nn.2897>.
- Scheckel, C., Drapeau, E., Frias, M.A., Park, C.Y., Fak, J., Zucker-Scharff, I., Kou, Y., Haroutunian, V., Ma'ayan, A., Buxbaum, J.D., and Darnell, R.B. (2016). Regulatory consequences of neuronal ELAV-like protein binding to coding and non-coding RNAs in human brain. *Elife* 5, e10421. <https://doi.org/10.7554/eLife.10421>.
- Schneider, J.W., Gao, Z., Li, S., Farooqi, M., Tang, T.S., Bezprozvanny, I., Frantz, D.E., and Hsieh, J. (2008). Small-molecule activation of neuronal cell fate. *Nat. Chem. Biol.* 4, 408–410. <https://doi.org/10.1038/nchembio.95>.
- Victor, M.B., Richner, M., Hermansteyne, T.O., Ransdell, J.L., Sobieski, C., Deng, P.Y., Klyachko, V.A., Nerbonne, J.M., and Yoo, A.S. (2014). Generation of human striatal neurons by MicroRNA-dependent direct conversion of fibroblasts. *Neuron* 84, 311–323. <https://doi.org/10.1016/j.neuron.2014.10.016>.
- Victor, M.B., Richner, M., Olsen, H.E., Lee, S.W., Monteys, A.M., Ma, C., Huh, C.J., Zhang, B., Davidson, B.L., Yang, X.W., and Yoo, A.S. (2018). Striatal neurons directly converted from Huntington's disease patient fibroblasts recapitulate age-associated disease phenotypes. *Nat. Neurosci.* 21, 341–352. <https://doi.org/10.1038/s41593-018-0075-7>.
- Visvanathan, J., Lee, S., Lee, B., Lee, J.W., and Lee, S.K. (2007). The microRNA miR-124 antagonizes the anti-neural REST/SCP1 pathway during embryonic CNS development. *Genes Dev.* 21, 744–749. <https://doi.org/10.1101/gad.1519107>.
- Vogel, K.U., Bell, L.S., Galloway, A., Ahlfors, H., and Turner, M. (2016). The RNA-binding proteins Zfp361l and Zfp3612 enforce the thymic β -selection checkpoint by limiting DNA damage response signaling and cell cycle progression. *J. Immunol.* 197, 2673–2685. <https://doi.org/10.4049/jimmunol.1600854>.
- Volvert, M.L., Prévot, P.P., Close, P., Laguesse, S., Pirotte, S., Hemp-hill, J., Rogister, F., Kruzy, N., Sacheli, R., Moonen, G., et al. (2014). MicroRNA targeting of CoREST controls polarization of migrating cortical neurons. *Cell Rep.* 7, 1168–1183. <https://doi.org/10.1016/j.celrep.2014.03.075>.
- Wang, L.L., Serrano, C., Zhong, X., Ma, S., Zou, Y., and Zhang, C.L. (2021). Revisiting astrocyte to neuron conversion with lineage tracing in vivo. *Cell* 184, 5465–5481.e16. <https://doi.org/10.1016/j.cell.2021.09.005>.
- Weng, Q., Wang, J., Wang, J., He, D., Cheng, Z., Zhang, F., Verma, R., Xu, L., Dong, X., Liao, Y., et al. (2019). Single-cell transcriptomics uncovers glial progenitor diversity and cell fate determinants during development and gliomagenesis. *Cell Stem Cell* 24, 707–723.e8. <https://doi.org/10.1016/j.stem.2019.03.006>.
- Weyn-Vanhenenryck, S.M., Mele, A., Yan, Q., Sun, S., Farny, N., Zhang, Z., Xue, C., Herre, M., Silver, P.A., Zhang, M.Q., et al. (2014). HITS-CLIP and integrative modeling define the Rbfox splicing-regulatory network linked to brain development and autism. *Cell Rep.* 6, 1139–1152. <https://doi.org/10.1016/j.celrep.2014.02.005>.
- Wu, Z., Parry, M., Hou, X.Y., Liu, M.H., Wang, H., Cain, R., Pei, Z.F., Chen, Y.C., Guo, Z.Y., Abhijeet, S., and Chen, G. (2020). Gene therapy conversion of striatal astrocytes into GABAergic neurons in mouse models of Huntington's disease. *Nat. Commun.* 11, 1105. <https://doi.org/10.1038/s41467-020-14855-3>.
- Yang, C., Iyer, R.R., Yu, A.C.H., Yong, R.L., Park, D.M., Weil, R.J., Ikejiri, B., Brady, R.O., Lonser, R.R., and Zhuang, Z. (2012). β -catenin signaling initiates the activation of astrocytes and its dysregulation contributes to the pathogenesis of astrocytomas. *Proc. Natl. Acad. Sci. USA* 109, 6963–6968. <https://doi.org/10.1073/pnas.1118754109>.
- Yeom, K.H., Mitchell, S., Linares, A.J., Zheng, S., Lin, C.H., Wang, X.J., Hoffmann, A., and Black, D.L. (2018). Polypyrimidine tract-binding protein blocks miRNA-124 biogenesis to enforce its neuronal-specific expression in the mouse. *Proc. Natl. Acad. Sci. USA* 115, E11061–E11070. <https://doi.org/10.1073/pnas.1809609115>.
- Yoo, A.S., Staahl, B.T., Chen, L., and Crabtree, G.R. (2009). MicroRNA-mediated switching of chromatin-remodelling complexes in neural development. *Nature* 460, 642–646. <https://doi.org/10.1038/nature08139>.
- Yoo, A.S., Sun, A.X., Li, L., Shcheglovitov, A., Portmann, T., Li, Y., Lee-Messer, C., Dolmetsch, R.E., Tsien, R.W., and Crabtree, G.R. (2011). MicroRNA-mediated conversion of human fibroblasts to neurons. *Nature* 476, 228–231. <https://doi.org/10.1038/nature10323>.



Yuzwa, S.A., Borrett, M.J., Innes, B.T., Voronova, A., Ketela, T., Kaplan, D.R., Bader, G.D., and Miller, F.D. (2017). Developmental emergence of adult neural stem cells as revealed by single-cell transcriptional profiling. *Cell Rep.* *21*, 3970–3986. <https://doi.org/10.1016/j.celrep.2017.12.017>.

Zhang, Y., Chen, K., Sloan, S.A., Bennett, M.L., Scholze, A.R., O’Keeffe, S., Phatnani, H.P., Guarnieri, P., Caneda, C., Ruderisch, N., et al. (2014). An RNA-sequencing transcriptome and splicing

database of glia, neurons, and vascular cells of the cerebral cortex. *J. Neurosci.* *34*, 11929–11947. <https://doi.org/10.1523/JNEUROSCI.1860-14.2014>.

Zhou, H., Su, J., Hu, X., Zhou, C., Li, H., Chen, Z., Xiao, Q., Wang, B., Wu, W., Sun, Y., et al. (2020). Glia-to-Neuron conversion by CRISPR-CasRx alleviates symptoms of neurological disease in mice. *Cell* *181*, 590–603.e16. <https://doi.org/10.1016/j.cell.2020.03.024>.